Earth Systems and Environment (2025) 9:801–824
https://doi.org/10.1007/s41748-025-00605-2

ORIGINAL ARTICLE

Soil Moisture Satellite Data Under Scrutiny: Assessing Accuracy Through Environmental Proxies and Extended Triple Collocation Analysis

Angelika Pataki[1] · László Bertalan[1,2] · László Pásztor[3,4] · Loránd Attila Nagy[1] · Dávid Abriha[1] · Shunlin Liang[5] · Sudhir Kumar Singh[6] · Szilárd Szabó[1,2]

Received: 22 May 2024 / Revised: 13 January 2025 / Accepted: 14 February 2025 / Published online: 26 February 2025

Abstract

16 different satellite soil moisture (SM) datasets (passive, active, combined, and model data) were compared at the European scale. We hypothesized that SM should be reflected by a variety of environmental factors, such as topography, hydroclimatology, soil characteristics, and biomass. Robust correlation was used to explore the relationship among the satellite data products, and the Recursive Feature Elimination method combined with the Random Forest Regression (RFR) algorithm was used to find the most important variables. Variations in SM-values were analyzed using extended triple collocation analysis (ETC), while the accuracy metrics of the RFR models were summarized through UMAP dimension reduction. The result showed that generally, correlations among the SM products were low ($r<0.5$) with some exceptions. GLDAS had the weakest correlation with the other SM products. Using SM as the dependent variable in regression models, model testing showed that GLDAS's SM was explained with the highest accuracy based on the Nash-Sutcliffe Efficiency (0.631), followed by the SMOPS (0.624). SSM demonstrated the lowest environmental influence (NSE: 0.288). Using UMAP, ETC, it was determined that SMOPS exhibited superior performance in terms of error variance and model accuracy; however, based on the ETC results, GRD.P was deemed the most suitable option. Results called the attention of varying SM values by products, being biased by various environmental factors and the applied technology of the satellites.

Keywords Correlation · Environmental Factors · Satellite Sensors · Soil Moisture · Statistical Modeling

1 Introduction

Soil moisture (SM) is part of the hydrological cycle and the global water cycle (Seneviratne et al. 2010) among the 50 most important climate factors (GCOS-138 2010). Changes in SM can affect temperature anomalies (Fischer et al. 2007; Jaeger and Seneviratne 2011), weather and climate conditions (Entekhabi et al. 1996). In drought-prone areas, monitoring SM is very important as it can affect the water balance of agricultural crops (Dai 2011). SM is represented in different climate models, such as GFS (Zheng et al. 2018), ECMWF (Albergel et al. 2012), and ICON (Reinert et al. 2021). Furthermore, SM is also important input data in hydrological modeling (Saxe et al. 2021), soil-water management (Dobriyal et al. 2012), soil-water profile modeling (Heathman et al. 2003), precipitation estimation (Pellarin et al. 2013) and drought analysis (Sheffield 2004; Kamalanandhini 2023). Understanding the spatial and

✉ László Bertalan
bertalan@science.unideb.hu

1 Department of Physical Geography and Geoinformation Systems, University of Debrecen, H- 4032 Egyetem tér 1, Debrecen, Hungary

2 National Laboratory for Water Science and Water Safety, University of Debrecen, Egyetem tér 1, Debrecen H-4032, Hungary

3 Institute for Soil Sciences, HUN-REN Centre for Agricultural Research, Herman Ottó út 15, Budapest 1022, Hungary

4 National Laboratory for Water Science and Water Safety, Herman Ottó út 15, Budapest 1022, Hungary

5 Jockey Club Laboratory of Quantitative Remote Sensing, Department of Geography, University of Hong Kong, Hong Kong, China

6 Nehru Science Centre, K. Banerjee Centre of Atmospheric and Ocean Studies, IIDS, University of Allahabad, Allahabad 211002, UP, India

temporal distribution of soil moisture (SM) values is crucial for optimizing irrigation practices, ultimately enhancing agricultural efficiency and augmenting crop yields (Hanson et al. 2000; Schmeller et al. 2022). The quantification of soil water content and moisture within distinct soil layers is essential for monitoring and estimation of evapotranspiration (Zhang and Schilling 2006; Li et al. 2009; Musyimi et al. 2022). The reconstruction of temporal and spatial variability in SM, crucial for the optimal development of vegetation, significantly influences plant growth dynamics, as elucidated by studies such as those conducted by Kramer (1944) and Veihmeyer and Hendrickson (1950). The importance of SM in agriculture has been extensively studied and widely acknowledged, as evidenced by numerous recent investigations (Liao et al. 2021; Meng et al. 2021; Togneri et al. 2022). Consequently, the scientific investigation of this phenomenon assumes paramount importance due to its fundamental role in ensuring food supply within agricultural systems.

Various methodologies exist for assessing soil moisture (SM), with the gravimetric method (Mukhlisin et al. 2021) being the most prevalent. This approach involves measuring SM through the drying and subsequent weight loss of soil samples, and its significance is underscored by its widespread application for calibration purposes, as exemplified by (Reynolds 1970). Contemporary methodologies for SM measurement encompass a range of devices and sensors, including but not limited to tensiometers, granular matrix sensors, time domain reflectometry (TDR) equipment, frequency domain reflectometry (FDR) equipment, and prolonged deployment SM measuring devices (Rasheed et al. 2022; Moret-Fernández et al. 2022) such as VH400. These instruments are strategically embedded within specific soil layers for extended durations, facilitating the acquisition of frequent and precise SM measurements (Garg et al. 2016). International networks dedicated to SM measurement, such as the ISMN (International SM Network), comprise a total of 71 networks and 2842 stations, predominantly distributed in the northern hemisphere (Dorigo et al. 2021a), or domestic networks such as the Australian OzNet, CosmOz, OzFlux (Bhardwaj et al. 2022), the French SMOSMANIA (Soil Moisture Observing System - Meteorological Automatic Network Integrated Application) (Calvet et al. 2007) or the Mongolian NAQU (NAQU Network) (Chen et al. 2013). SM estimation can be achieved indirectly using various sensors mounted on Unmanned Aerial Systems (UAS), including multispectral and thermal cameras, offering high-resolution data over limited spatial extents. This method can be supplemented by gravimetric and TDR methods (Paruta et al. 2021). UAS-based measurements demonstrate effectiveness when targeting small-scale field extents (Bertalan et al. 2022). Alternatively, for monitoring extensive areas satellite-derived data may prove more suitable.

Several methods exist for estimating SM using optical satellite data along with various spectral indices (Todd and Hoffer 1998; Ghasemloo et al. 2022), as well as multi-factor models like the OPTRAM model (Ambrosone et al. 2020; Babaeian et al. 2018; Li et al. 2021). However satellite data presents challenges, including occasional gaps resulting from satellite time drift (Wang et al. 2012) and limitations in spatial resolution. Some SM datasets exhibit spatial resolutions as low as several tens of kilometers, as observed in studies by (Beck et al. 2021; Zheng et al. 2022; Bhardwaj et al. 2022; Liu et al. 2012b). Despite these drawbacks, the advantage lies in the extensive temporal coverage and global spatial representation, enabling a comprehensive overview of SM variation on the global scale.

SM assessment can be conducted using either active or passive sensors too. In vegetated areas, passive remote sensing exhibits a greater diminution of sensitivity compared to scattering models, with active remote sensing proving more resilient in this context, as elucidated by (Fung and Eom 1985). Du et al. (2000) conducted a comprehensive study utilizing both scattering and emission models, incorporating both L-band passive and active methodologies. Their findings indicate that radiometric sensitivity decreases with increasing vegetation thickness concerning SM. Furthermore, both radiometric and radar sensitivity showed comparable reductions with increasing vegetation thickness on bare soil surfaces. Additionally, the angle of incidence during measurement emerges as a factor influencing the uncertainty in active SM measurement (Crow et al. 2010). In radar-based SM measurements, the impact of surface roughness is a critical consideration, affecting backscattering. Consequently, when parameterizing SM data obtained through radar, incorporating a correction for roughness becomes imperative to mitigate uncertainties in the SM values (Jackson et al. 1997; Mira et al. 2022; Zheng et al. 2021; Verhoest et al. 2008).

The determination of SM is subject to modification by a number of influencing factors, including the hydrological properties of the soil, i.e., the spatial movement and vertical position of groundwater, exerting an impact on both the SM within the root zone and surface evapotranspiration (Chen and Hu 2004; Blanka-Végi et al. 2025). SM dynamics are also influenced by vegetation, with grasslands exhibiting decreased SM due to evapotranspiration (Zhang and Schilling 2006). In vegetated areas, the accuracy of radar readings is constrained when SM values fall below 50%, while within the range of 50–150%, an observed error of ±15% occurs in 90% of cases (Ulaby et al. 1982). Spatial variation in SM, as detailed by (Wang et al. 2018), correlates with spatial fluctuations in plant cover. An inverse relationship

between temperature and SM variation was described by the study of Lakshmi et al. (2003), which observed that SM decreases with rising temperature post-precipitation. Yang et al. (2022) concluded that precipitation significantly influences SM replenishment in Xinjiang based on data obtained between 1985 and 2015. In addition, (Kerr 2007) underscored the complexity of satellite-based SM measurements in the context of frozen ground surfaces, topography, urban areas, trees, and vegetation that absorbs precipitation.

The considerations of accuracy and validation are pivotal, given the impact on the usability of such data. Typically, accuracy testing and validation involve comparisons with in-situ networks and other SM datasets (Qiu et al. 2016; Holgate et al. 2016; Ford and Quiring 2019; Ma et al. 2019; Mazzariello et al. 2023). Despite the abundance of satellite-based SM information, validation encounters challenges related to resolution. Spatial resolutions of 1–5 km products cover extensive areas (Sure and Dikshit 2022; Zhang et al. 2023), and a ground monitoring network reliant on point-based measurements may not accurately represent values applicable to larger scales, such as 100-500-2500 hectares. While large homogenous areas can yield acceptable data, identifying suitable land segments in the necessary quantity for evaluation can still be challenging. Accordingly, the temporal aspect is also crucial, particularly when surface SM undergoes rapid changes in warm weather conditions with clear skies. All satellite products are validated, with numerous studies presenting accuracies, but the use of multiple products to characterize the SM of a specific area may yield varying results. This raises the question of which product aligns more closely with the real SM. Over the past decade, numerous SM products have been developed and operated, prompting several comparative analyses among these datasets. However, such analyses typically involve the comparison of only 2–3 products. The comparison of different SM data is of importance, necessitating a thorough assessment of errors or uncertainties before their appropriate utilization. Accordingly, a comprehensive comparison of existing satellite-derived SM products becomes paramount, particularly in evaluating values, seasonal dependencies and their influence on topography, climatic conditions and soil variables.

We performed a comparison among several satellite SM products on a continental scale, addressing the following hypotheses. We assumed that (i) SM values should exhibit similarly across different SM products, (ii) SM values should reflect environmental factors such as climatic region, meteorological factors, topographic features, soil properties, and biomass. Accordingly, we compared the SM datasets and modeled SM across Europe, expecting that modelled SM would demonstrate a high explained variance with low model errors. Our hypothesis suggested that environmental factors, when employed as predictors in a modeling framework, should ensure a good fit with the SM as the target variable. Specifically, higher R^2 and lower Root Mean Square Error (RMSE) indicate good response, which consequently reflects the reliability of the SM data. We hypothesized that a multivariate evaluation of accuracy metrics aligns with the error variance derived from triple collocation analysis.

2 Materials and Methods

2.1 Study Area

Europe was selected as the study area (Fig. 1), due to the necessity of a continental scale for unveiling the spatial patterns of the SM, driven by the typically low spatial resolution of the datasets (1–25 km; Supplement 1). Furthermore, the diverse topography and climate across Europe were considered, with the expectation that these variations would be manifest in the observed SM values.

2.2 Satellite Data

We incorporated 16 distinct SM data products in the analysis, each characterized by unique features (Supplement 1). SM products AMSR2, ESA, and GRD had three variations each, therefore, finally, we evaluated 16 products. For all instances, the data were obtained for, focusing on the vegetation period, 01.04.2020, 01.06.2020, and 01.08.2020 or the nearest available date with optimal spatial resolution. Additionally, surface SM data was captured within the top 5–10 cm, depending on the specific product.

2.3 Datasets

2.3.1 Active Microwave Products

The SSM (Surface Soil Moisture) data product was derived using Sentinel-1 satellite data (Bauer-Marschallinger et al. 2017, 2018; Doubkova et al. 2016). The estimated relative SM values are expressed as a percentage ranging from 0 to 100% in terms of saturation. It should be noted that the SSM is not capable of accurately quantifying SM in regions characterized by extremely dry conditions, frozen ground, snow-covered ground, dense vegetation, and flooding. However, it is deemed suitable for application in areas devoid of frost and snow, featuring low vegetation, and areas exhibiting minimal relief (Bauer-Marschallinger 2019).

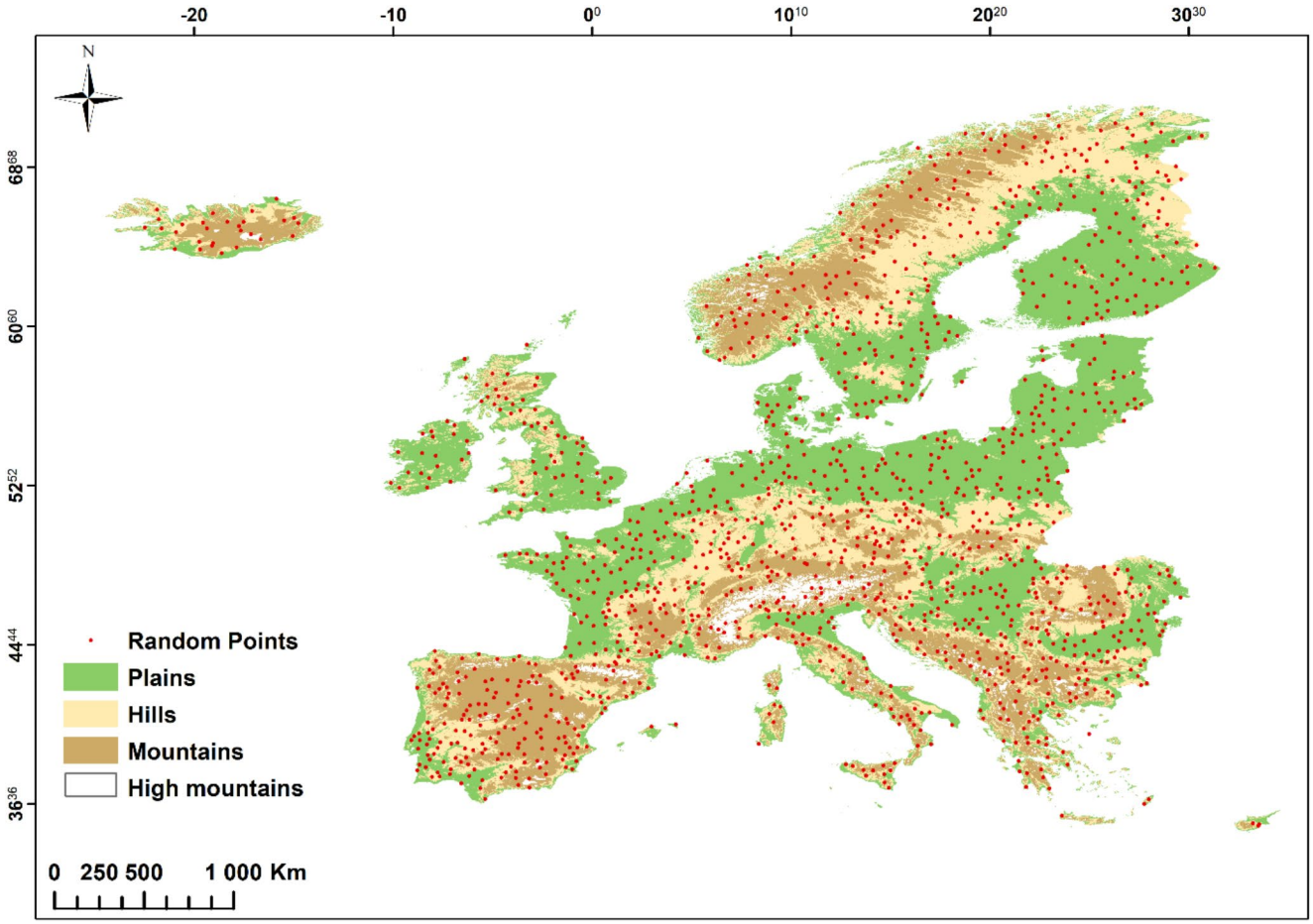

Fig. 1 Topography and distribution of random sampling points within the study area

2.3.2 Passive Microwave Products

The AMSR2 sensor (Advanced Microwave Scanning Radiometer 2), is the decessor of the AMSR-E sensor (Bhardwaj et al. 2022; Kim et al. 2015). The SMAP (Soil Moisture Active Passive) satellite primarily serves the purpose of monitoring SM and detecting frozen/thawed surfaces. While equipped with both a radiometer and a radar, it is noteworthy that the radar component experienced a malfunction in July 2015. Consequently, the radar data has been substituted with data obtained from the Sentinel-1 satellite (Colliander et al. 2017). SMOS (Soil Moisture and Ocean Salinity) provides data for SM and ocean surface salinity studies through its radiometer (Bhardwaj et al. 2022). SMOS-IC (INRA-CESBIO) is a product that includes L-band vegetation optical depth supplementary data (Fernandez-Moran et al. 2017; Wigneron et al. 2021). In the case of AMSR2 data, we utilized the Land Parameter Retrieval Model (LPRM) algorithm (Kim et al. 2016; Owe et al. 2008), derived from SMAP L3 level data, involves fusion into a two-layer Palmer model, and Ensemble Kalman Filter is employed for data assimilation (Sazib et al. 2022). Both AMSR2 and SMOS. BEC and SMOS.IC data are subdivided into ascending and descending datasets. For AMSR2, SMAP and SMOS. BEC, the utilization of brightness temperature, vegetation, land surface temperature, or soil temperature parameters is common (Kim et al. 2015; Portal et al. 2017; O'Neill et al. 2020). The SMAP L2/L3 algorithm incorporates soil texture, water, forest, urban, upland, and land masks in its processing (O'Neill et al. 2020).

2.3.3 Combined Products

The ESA CCI (ESA Climate Change Initiative Program) and Gridded Data combine three types of data, active, passive, and combined (Dorigo et al. 2015, 2021b; Gruber et al. 2019). The SMOPS (Soil Moisture Operational Products System) is composed of several components (ESA SMOS, ASCAT, AMSR2, SMAP), which are available separately or as a combined layer (Liu et al. 2016; Yin et al. 2022). The ESA CCI and Gridded Data repositories incorporate multiple types of SM datasets, exhibiting considerable similarities. Both repositories calculate data from a range of sources, including ASCAT, AMI-WS, AMSR-E, AMSR2,

GLDAS, SMAP, SMOS, SMMR, SSM/I, TMI, and WindSat. Moreover, ESA CCI uses GMI, and MWRI data, while Gridded Data incorporates GLWD, GTOPO30, and ISMN data. Regions with data gaps or limited data availability, areas typically observed in rainforests, and areas covered by snow. To address this Gridded Data employs a snow cover estimator or frozen ground layer is used as supplementary data (Dorigo et al. 2021b; Scanlon et al. 2021). In contrast, the SMOPS utilizes various inputs, including soil texture, surface cover data, NRT SMOS L1C brightness temperature, and NDVI values, among others (Zhan et al. 2016).

2.3.4 Model Product

The GLDAS (Global Land Data Assimilation System) integrates satellite data and ground observations, employing three land surface models: Mosaic, Noah, CLM, and VIC (Spennemann et al. 2015). The model incorporates various influencing factors, including vegetation data, elevation, Leaf Area Index, and several soil parameters such as texture, soil porosity, soil color, and fractions of clay, sand, and silt. SM measurements are conducted in multiple soil layers, spanning both the surface and the root zone, expressed in units of kg/m^2 (Rodell et al. 2004; Sun et al. 2022). ERA5-Land is the 5th generation land product of European ReAnalysis, from the Copernicus Climate Change Service. ERA5-Land is produced using the ECMWF climate model and therefore includes a significant number of variables in addition to the volumetric soil water layers, i.e. evaporation, precipitation, surface pressure, leaf area index, temperature, and wind parameters (Copernicus Climate Change Service 2019; Diouf et al. 2020; Muñoz-Sabater et al. 2021).

2.4 SM Data Accuracy

SSM was compared with the absolute SM content obtained at in-situ measurement stations. For the results, the target accuracy is 0.04 m^3/m^3 but this was achieved only in 2 cases by SSM (Bauer-Marschallinger 2018). A low agreement between the reference data from the stations and the SSM values was observed, i.e. median $R = 0.29$ and mean RMSD (Root Mean Square Deviation) = 0.088 m^3/m^3 (Bauer-Marschallinger et al. 2019). Wen et al. (2014) concluded that the accuracy of GLDAS Noah, for the top 10 cm of soil, was overestimated compared to the CEOP Mongolian network data, with RMSE = 0.132. Based on the NAQU Network concluded in the lower soil layers (10–40 cm), the land surface models of GLDAS Noah and CLM represent the moisture well but underestimate the surface SM. In this case, the RMSE varies from 0.02 to 0.14 m^3/m^3 depending on the depth and land surface model (Chen et al. 2013). Seongkyun et al. (2016) examined the different bands of AMSR2 and concluded that in ascending mode, the X-band data gave better results than the C1 and C2 band data. The accuracy target for AMSR2 is a value is less than 0.08 m^3/m^3. This value was between 0.07 for the X band and 0.07 and 0.09 for the C bands (Yee et al. 2017). For AMSR2 data, it was found that it cannot detect low SM values well (Unnikrishnan et al. 2016).

The fundamental objective of the SMAP project is to estimate the SM value for the upper 5 cm of soil, aiming for a volumetric error of not exceeding 0.04 cm^3/cm^3. This expectation holds, with exceptions for areas characterized by vegetation with water content exceeding 5 kg/m^2, urban areas, mountainous, frozen, snow- and ice-covered areas, as well as water surfaces (O'Neill et al. 2010). Based on the analysis of data from the core validation sites, SMAP PE (Enhanced radiometer-based) and P (Radiometer-based) yielded average unbiased Root Mean Square Deviation (ubRMSD) results below 0.04 m^3/m^3, even under different algorithms (Colliander et al. 2022).

The L3 and L4 level products of SMOS.BEC underwent an examination in representative regions of Spain and Brazil, wherein they were compared with data from the REMEDHUS and CEMADEN in-situ measurement networks within semi-arid contexts. SMOS. BEC L4 data show correlation values surpassing 0.6, a trend mirrored in L3 data as well (Spatafora et al. 2020). In the case of SMOS.IC Version 2 validation was performed using modelled ECMWF SM values, the SMOSMANIA, and ORACLE network values. The overall value of ubRMSD was 0.055 m^3/m^3 (Li et al. 2020).

In terms of accuracy assessment, the combined ESA CCI v6.1 and v5.2 data have been validated with ERA5 SM data spanning the period 2007–2019. The outcomes reveal relatively low correlation values for northern latitudes and areas characterized by bare soils (Scanlon 2021). The combined ESA CCI v6.1 and v5.2 data compared to the ISMN (International Soil Moisture Network) data show correlation coefficient values of 0.613 (v5.2) and 0.644 (v6.1), for the active data it is 0.487 (v5.2), 0.554 (v6.1), for the passive data it is 0.599 (v5.2), 0.618 (v6.1) (Hirschi et al. 2021). In terms of accuracy, the SMOPS, in its current version (version 3.0) exhibits an average ubRMSE of 0.059 m^3/m^3, validated against SCAN SM values (Yin et al. 2020). In an independent accuracy assessment, Gridded Data underwent comparison with in-situ SM data, considering the different conditions. The correlations between the datasets generally exceeded 0.4 and 0.8. In terms of accuracy, the ubRMSD remains below 0.10 m^3/m^3 for all conditions tested. However, it is noteworthy that the anticipated accuracy target of 0.04 m^3/m^3 is not consistently achieved across all conditions (Dorigo et al. 2021c). The performance of ERA5-Land has been tested in several sample areas, i.e., European, African, and Australian sample areas, and it has been concluded that

ERA5-Land performs better than ERA5 (Muñoz-Sabater et al. 2021).

2.5 Environmental Factors

We employed a modeling approach to estimate SM values, incorporating environmental factors such as climatic, soil, and topographic factors, along with biomass considerations. The following factors were considered in the models: climate factors (sum of precipitation and temperature 1–7 days prior to the date of data collection, mean maximum temperature 1–7 days prior to the date of data collection, Köppen climatic regions), soil-related factors (water content, soil texture, sand content, clay content), topographic factors (13 geomorphometric indices and topographic categories); and the NDVI (for details see (Supplement 2).

2.6 Data Processing

For data analysis, random points were generated across Europe, ensuring a minimum distance of 25 km between each point, justified by the coarsest spatial resolution of the involved data. Consequently, 1,454 random points were generated (Fig. 2). Subsequently, each SM dataset was converted to m^3/m^3 as a standardized unit. The distribution of random points aligned with the Köppen-Geiger climate classification yielding the following counts: B:73, C:569, D:765, E:47. Similarly, with respect to DEM categories, the points are distributed among plains: 669, hills: 421, mountains: 340, high mountains: 24. The number of points represented the extent of climatic zones and topography, and were the basis of generating a dataset, extracting the pixel values of the given locations from the maps of the SM-products and environmental factors.

2.7 Comparison and Statistical Modeling

2.7.1 Comparison of the Satellite SM Data

According to the Shapiro-Wilk test, the SM data usually did not follow the normal distribution; thus, we used the robust Winsorized Pearson correlation coefficient to reveal the relationship between the satellite SM source pairs (using 5% for trimming the outliers) (Dunn and Smyth 2018) using

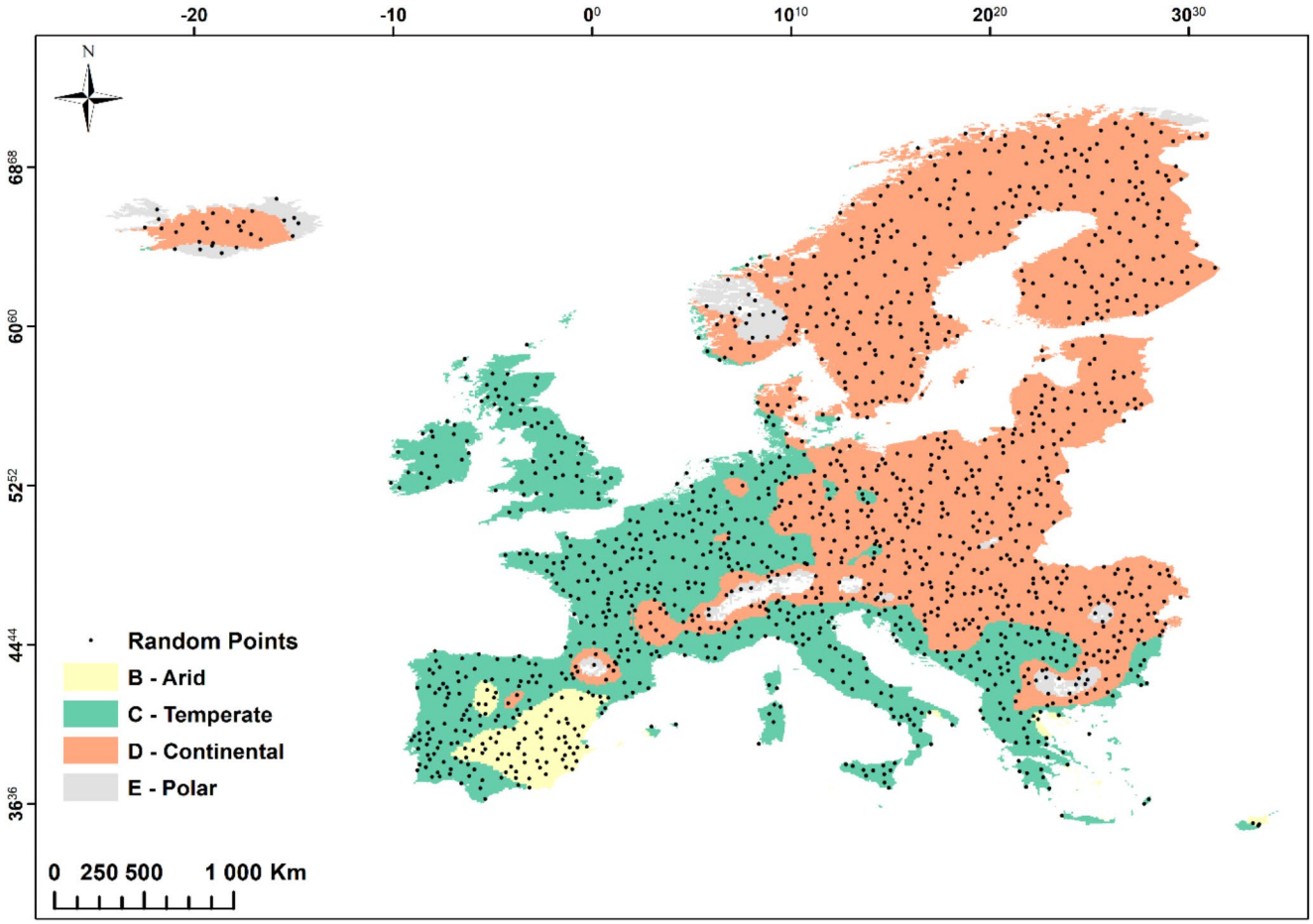

Fig. 2 Map of Köppen-Geiger climate classification with the random points

the ggstatsplot (Patil 2021) package in R. Correlation matrices of SM products were compared with the Mantel test by Köppen and topographic zones, and by dates of data collection (Bakker 2024).

Assuming that the SM products had independent errors, we employed the Triple Collocation Analysis (TCA) to estimate the variance of noise error (errVar). To obtain the desired results, we utilized the Extended Triple Collocation (ETC), a modified version developed by McColl et al. (2014). ETC calculates both errVar and an additional measure, the squared correlation to the unknown (i.e., conceptual) true values (rho2), as a scaled, unbiased signal-to-noise ratio. We rebuilt the original Matlab code in the R environment and extended it to process any number of input variables. By forming triplets from the input variables in all possible combinations, we calculated the errVar and rho2 values. In our case, with 16 SM products, we had 560 variations. The results were summarized by mean SMs in diagrams where favorable outcomes exhibited low Mean_errVar (mean error variance) indicating low random error (consistency), and high Mean_rho2 (mean rho2s) indicating low signal-to-noise error.

To evaluate the spatiotemporal significance of the data, we employed General Linear Modeling (GLM), incorporating the 'northing' and 'easting' coordinates as spatial parameters and the dates (April, June, August) to determine the relevance of the location and the date of data collection. In addition to statistical significance, we calculated the effect sizes (ω^2 as a standardized measure to express the magnitude of the effect) and adjusted R^2s (modified by the number of predictors) in R. ω^2 is the less biased measure of the effect size in GLMs (Lakens 2013), and values of 0.01 can be considered as small, 0.06 as medium, and >0.14 as a large effect (Field 2013).

Modelling was performed with the satellite SM sources (i.e., as target variables with the predictors of topographic variables, the Köppen climatic regions, NDVI, climatic and soil variables (according to Supplement 2). However, due to the high correlation of meteorological variables, first, we filtered out one of the most correlating pairs of predictors (SM values against the climatic variables), and finally, we used only the maximum temperature (sum of 7 days) and the precipitation of the previous day.

Random Forest Regression is a robust ensemble method in machine learning, and, unlike linear regression, there are no assumptions of normal distribution and homoscedasticity, making it a robust method. Several decision trees (usually hundreds) are being built parallel and each random tree uses a randomly chosen fraction of the training dataset. Furthermore, the variables involved in a given tree are also randomly chosen; the number of variables can be set by hyperparameter tuning or using the square root of all variables. Random sampling (bagging) in the training of the RFR model ensures avoidance of over-fitting.

Recursive Feature Elimination (RFE) was used to find the most important variables (selected predictors) combined with the RFR algorithm. Although RFR efficiently handles a large number of variables, it is advantageous to reduce the input variables, because it helps to eliminate the irrelevant and redundant variables, as well as to identify the most important ones. Some variables can act as noise in the models, therefore decreasing the model performance. RFE conducts models dropping the variable with the weakest contribution; finally, only one variable, having the largest contribution, remains. Most important variables are selected using an accuracy metric (depending on the tasks was a classification or regression), now we determined the most important input data using the lowest Root Mean Square Error (RMSE) (Chai and Draxler 2014).

During the modeling phase, we applied the RFR because of its efficiency and robustness (Forkuor et al. 2017; Liu et al. 2012a), and the input variables were the most important ones determined by the RFE for each SM product. RFR models were trained with 500 decision trees with random subsets of the training data. A hyperparameter tuning was performed with the number of variables at each node (mtry: from 1 to 20) with grid search within a 10-fold cross-validation (CV) with 3 repetitions. The final model was averaged and provided a better output than a single decision tree (Fig. 3). RFE and RFR model building was conducted in R 4.3.2 with the caret package (Kuhn 2008).

2.7.2 Model Evaluation

Our objective was to elucidate the structure of the most influential factors in remotely sensed SM data. Data were randomly split into training and testing subsets in 70:30% ratio with stratified random selection by climatic zones. The RFR was conducted on the training subset, then the model was applied to predict SM values with the testing subset.

First, we evaluated the minimums, lower quartiles, medians, upper quartiles, and maximums of the 30 models, the outputs of the model building with the CV method. Accuracy parameters were determined with the caret package of the R 4.3.2 (Kuhn 2008). For comparison with the literature, we also calculated the unbiased RMSE (ubRMSE) values of the models (Yang et al. 2020).

Independent testing with the testing subset was evaluated by the modelled and the observed values. Weighted R^2 (wR^2: weighted with gradient b), RMSE, ubRMSE, normalized RMSE (NMRSE), the Nash-Sutcliffe Efficiency (NSE), and the Kling-Gupta Efficiency (KGE) were determined to evaluate the accuracy. Accuracy metrics were determined

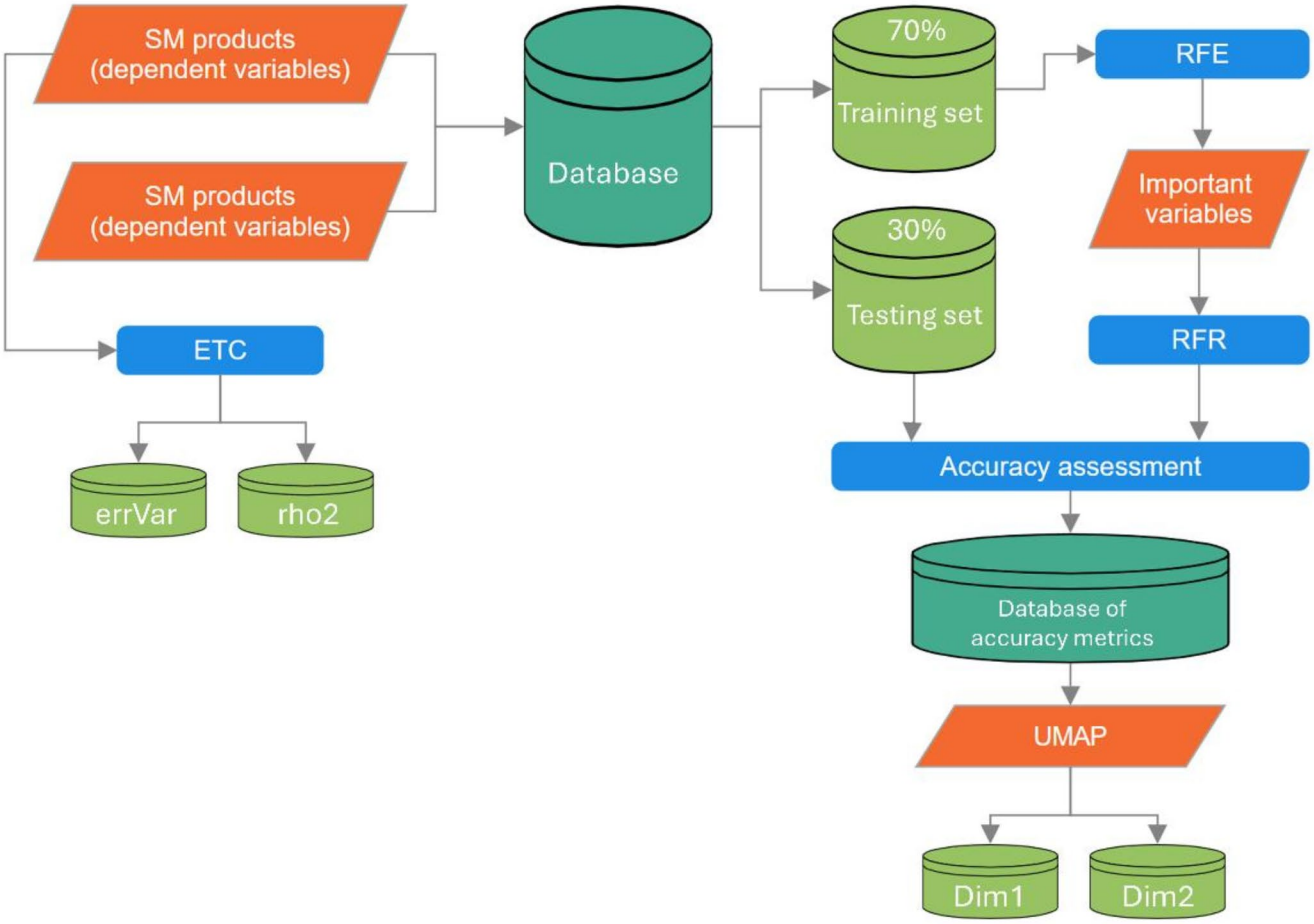

Fig. 3 Workflow of the SM product analysis and evaluation (ETC: Extended Triple Collocation; errVar: error variance, rho2: correlation coefficient, RFR: Random Forest Regression, UMAP: Uniform Manifold Approximation and Projection, Dim: dimension)

with the hidroGOF package of R (Mauricio Zambrano-Bigiarini 2024).

Lastly, we evaluated six different metrics for ranking the SM products, so we utilized a multivariate analysis to provide an overall synthesis of how these metrics contribute to the accuracy of the models collectively. To achieve this, we employed a multivariate model-based evaluation approach, which is a robust non-linear method, and the Uniform Manifold Approximation and Projection (UMAP) for dimensionality reduction. Prior to conducting the analysis, we normalized the accuracy metrics and set the number of neighbors to five to maintain the local structure of the data and investigate the clusters and patterns of the SM products. We subsequently visualized the results using UMAP, which was performed using the umap package in R (Konopka 2023).

3 Results

3.1 Analysis of SM Datasets

The SSM produced the highest values (0.69–0.82 m^3/m^3) for the medians for the relief categories, except for the high mountain category, where AMSR.C1 (0.79 m^3/m^3) showed the maximum medians (Fig. 4). Concerning median values, SMOS.IC exhibited the minimum for plain (0.08 m^3/m^3), mountains (0.05 m^3/m^3), and high mountains (0 m^3/m^3), while SMAP (0.06 m^3/m^3) recorded the minimum for hills. Analyzing the interquartile range (IQR), the widest ranges were found in all four cases for AMSR.X (0.41 m^3/m^3) for plains, 0.5 m^3/m^3 for hills, 0.48 m^3/m^3 for mountains and 0.78 m^3/m^3 for high mountains. Notably, combined data dominated for minimum values, with SMOPS (0.03 m^3/m^3) for the hills, GRD.C (0.04 m^3/m^3) for the mountains, GRD.P (0.04 m^3/m^3) as the passive data value for the plains, and SSM as the active data and SMOS.IC as the passive data (0 m^3/m^3) for the high mountains. In the comparison of relief

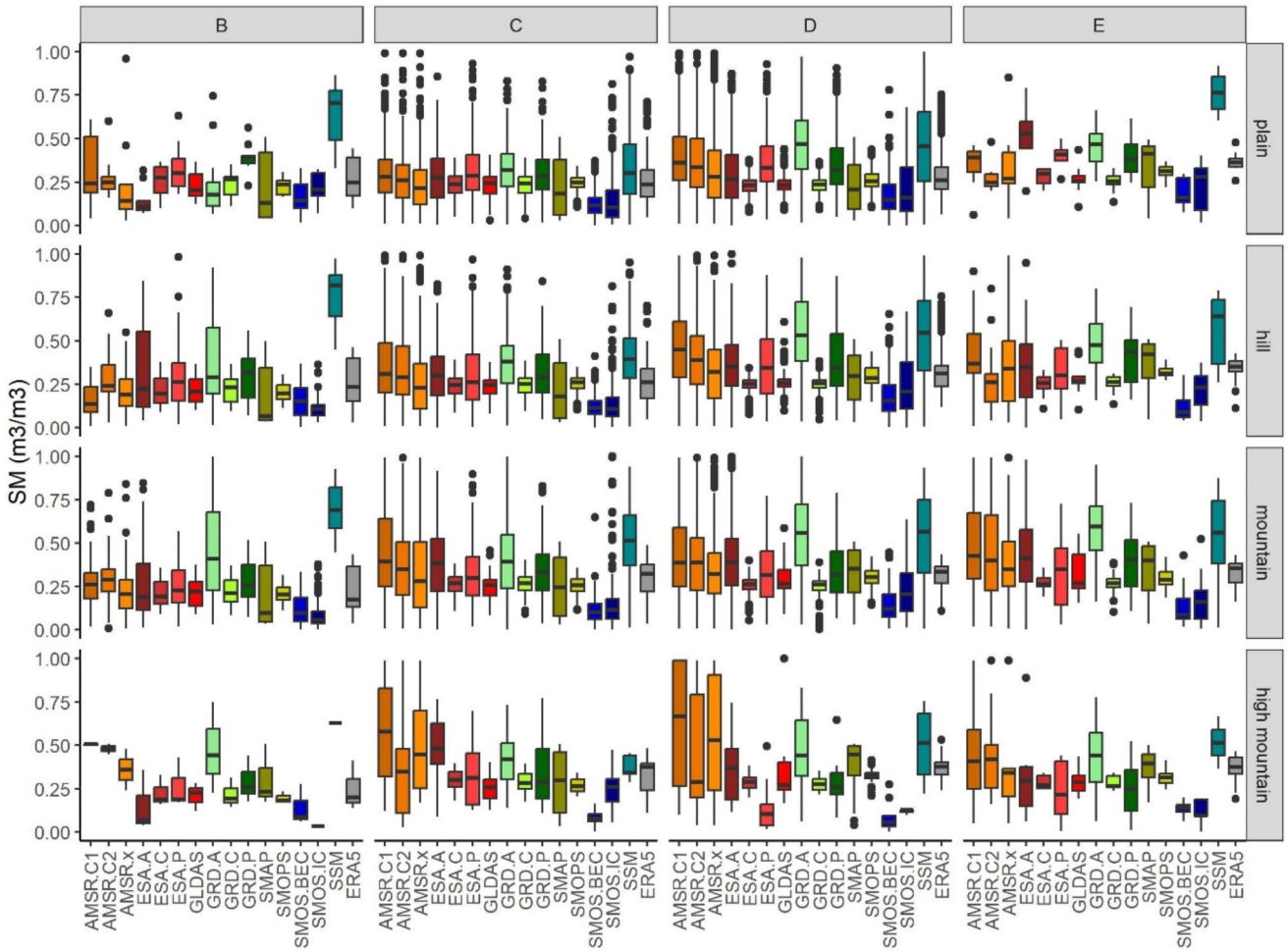

Fig. 4 The distribution of data from the SM sensors used

categories, medians displayed similar ranges across all four cases, whereas the high mountains exhibited a higher variance in the IQR.

In terms of the Köppen climate classes, the maxima of the medians were identified in three cases for SSM (B: 0.82 m^3/m^3; C: 0.51 m^3/m^3; E: 0.76 m^3/m^3) and in one cases for AMSR.C1 (D: 0. 79 m^3/m^3), while the minimum values were obtained by SMOS.IC (B: 0.03 m^3/m^3; D: 0 m^3/m^3) and SMOS.BEC (C: 0.07 m^3/m^3; E: 0.08 m^3/m^3). Regarding the IQR, the largest ranges were recorded in two cases by AMSR.X (D: 0.78 m^3/m^3; E: 0.5 m^3/m^3), while AMSR.C2 (0.54 m^3/m^3) in zone C and GRD.A (0.44 m^3/m^3) in zone B. Furthermore, for the minimum values, SMOPS (D: 0.03 m^3/m^3; E: 0.03 m^3/m^3) appears twice, the SSM and SMOS.IC (0 m^3/m^3) appears once in zone B and SMOS.BEC (0.04 m^3/m^3) once in climate zone C. For climate zones B and E, SSM was more significantly differentiated from the other models. The IQRs in zone D cover a significantly larger range than for the other three classes. Outliers are present in nearly all instances, with exceptions noted for high mountains and climatic zones B and C. In the cases of climatic zone E and high mountains, the dataset contained a relatively small number of elements, resulting in variations in the IQR of SM data.

Table 1 Standard deviation of the median SMs (m^3/m^3)

	Plain	Hill	Mountain	High mountain
B	0.139	0.165	0.149	0.181
C	0.066	0.082	0.103	0.113
D	0.102	0.117	0.117	0.211
E	0.143	0.128	0.129	0.113

Regarding the standard deviations of the medians across each category (Table 1), the optimal outcomes within zone C were observed for plains (0.066) and hills (0.082). Conversely, the least favorable results were noted in the high mountains category (B:0.181, D:0.211).

3.2 SM-values as Reflected in Spatiotemporal Parameters

The GLM indicated that both the date of data collection and the location had a significant impact on all SM products. Furthermore, the effect sizes varied. The easting, or the east-west situation of the sampling points, had only a small (or even negligible) effect with all SM products, with a negligible effect size of less than 0.005. In contrast, the northing, or the north-south situation, had the largest effect sizes among all the products, including ESA.P, SMPOS, and SMOS. BEC, and SMOS.IC. The date had a significant effect on AMSR.X and SMAP, with the largest effect sizes among all the factors. Notably, GLDAS was the only product with an effect size of less than 0.13 for both the date and the northing, as indicated in Supplement 3.

3.3 Correlations among the SM Data

The correlation analyses revealed instances of high correlation in only a few cases (Fig. 5), without exceptionally strong relationship in any of the cases. The closest relationship was observed for ESA.C and GRD.C (0.82) and ESA.P and GRD.P (0.8). Additional correlation values around 0.7 were noted between AMSR.C1 and AMSR.C2, AMSR.C2 and AMSR.X as well as ESA.A and GRD.A.

Values around 0.6 appeared for AMSR.X and AMSR.C1, GLDAS and ESA.C, GLDAS and SMAP, GRD.A and SSM. In other cases, lower correlation values were typical. The lowest correlation values were obtained for GLDAS, with 0.07 and 0.11.

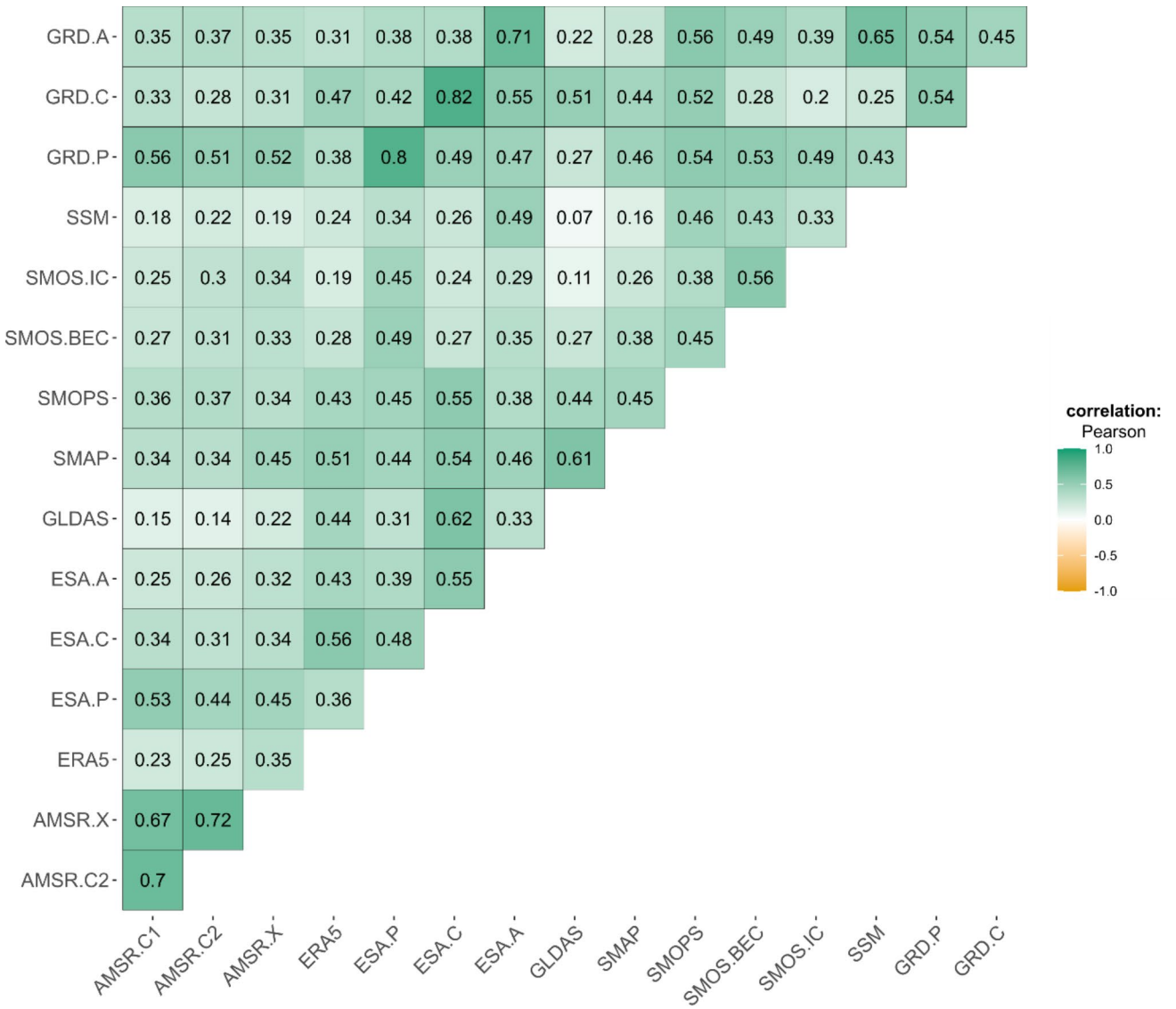

Fig. 5 Correlation structure between the SM products

3.4 The Correlations of SMs by the Köppen-Geiger Categories

Correlation exceeding 0.9 (Supplement 4) were observed only in the case of GRD.C and ESA.C (0.9) within zone B. Correlation values surpassing 0.8 were most prevalent in climate zone B (primarily involving ERA5, ESA.C, ESA.P, GRD.P, GRD.C, SMAP and SMOPS variations), followed by zone C (also for ESA.P and GRD.P, GRD.C, and ESA.C), and subsequently in zone D (with only one case: ESA.P and GRD.P). In zone E, there were 28 significant relationships out of 120 cases, primarily between ESA and GRD variations, with the highest correlation coefficient ($r>0.75$) observed for GRD.P and ESA.P, SMOS.IC and SMOS.BEC. However, the strength of each relationship diminished. Concurrently, there was a rise in the number of low correlation values, signifying minimal or no relationship between SM data in many cases. The majority of the non-significant values were identified in zone E (due to lower number of data), while only a few occurrences in other zones.

Based on the Mantel test, correlation matrices had varying relationships (Fig. 6). We compared the correlations based on the Köppen climate zones, topography, and dates. The Mantel test showed differences, especially in the case of ET and the high mountains having low similarities with the other zones. B, C, and D climate zones had moderate or higher similarities, while plains, hills, and mountains correlation matrices were of high similarities. Regarding the dates, April and August had only moderate similarity, while matrices of June and August and April and June had high similarities.

3.5 Structural Analysis of Environmental Factors as Covariates

RF models resulted in different accuracies by SM products, the lowest RMSE values were obtained for GLDAS, SMOPS, GRD.C, and ESA.C just below 0.05 m^3/m^3. The highest values were between 0.20 and 0.25 m^3/m^3 (AMSR.C1, AMSR.C2, AMSR.X, and SSM). For R^2, the lowest medians were revealed for SSM (0.25) and AMSR.C2 (0.29), while the highest ones belonged to the SMAP with a value of 0.63, GLDAS with 0.62 and SMOPS with 0.59 (Fig. 7).

In addition, an examination of the relationship between resultant and observed values was conducted. This analysis utilized metrics including nRMSE (Normalized Root Mean Square Error), ubRMSE, Kling-Gupta Efficiency (KGE), Nash-Sutcliffe Efficiency (NSE) and weighted R^2 (wR^2) (Fig. 8). The better performance of the model is characterized by the smallest nRMSE and ubRMSE values. The smallest nRMSE values were obtained for GLDAS (60.7), SMOPS (61.2) and SMAP (61.5), and for ubRMSE for SMOPS (0.03), ESA.C, GRD.C and GLDAS (0.04). The evaluation of model performance entailed the normalized assessment of NSE, while model efficiency was gauged using the KGE metric, and the model fit was tested using wR^2. Notably, superior outcomes were consistently associated with the SMOPS model (KGE: 0.640, NSE: 0.624, wR^2: 0.612), GLDAS model (KGE: 0.691, NSE: 0.631, wR^2: 0.614) and SMAP model (KGE: 0.673, NSE: 0.621, wR^2: 0.549). Conversely, inferior results were observed for SSM (KGE: 0.263, NSE: 0.288, wR^2: 0.236).

3.6 Accuracy Metrics and Triple Collocation

UMAP identified three clusters of the SM products, as indicated by the accuracy metrics (Fig. 8). The most accurate group comprised GLDAS, SMAP, SMOPS, GRD.P, and ERA5, while GRD.C, SMOS.BEC, and ESA.C were classified as the transition cluster. The lowest accuracy group consisted of AMSR.C1, AMSR.C2, ESA.A, ESA.P, SMOS.IC, GRD.A, and SSM, as shown in Fig. 9. It is worth noting that no discernible pattern was evident within the clusters based on the type of SM data.

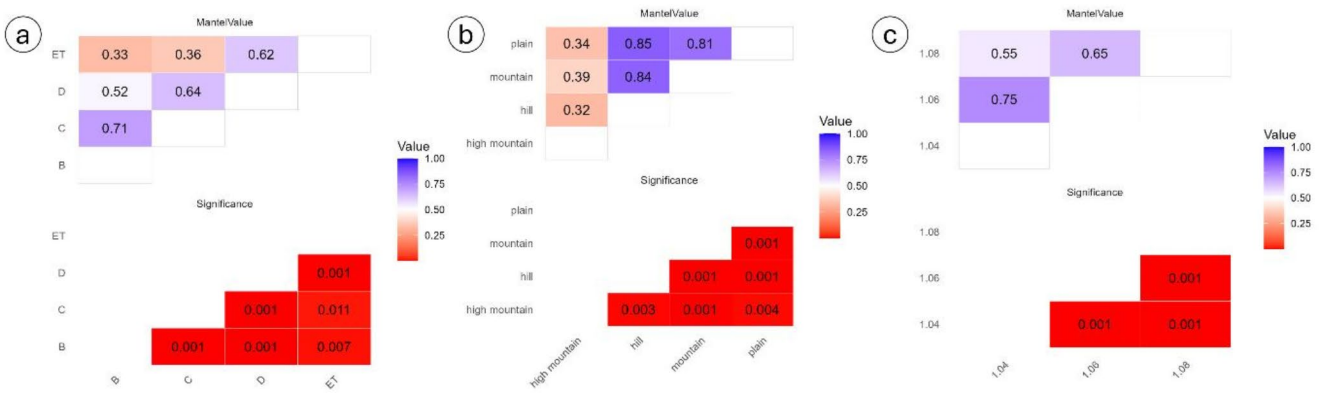

Fig. 6 Results of Mantel tests performed on the correlation matrices of the 16 SM products by Köppen and topographical zones, and dates

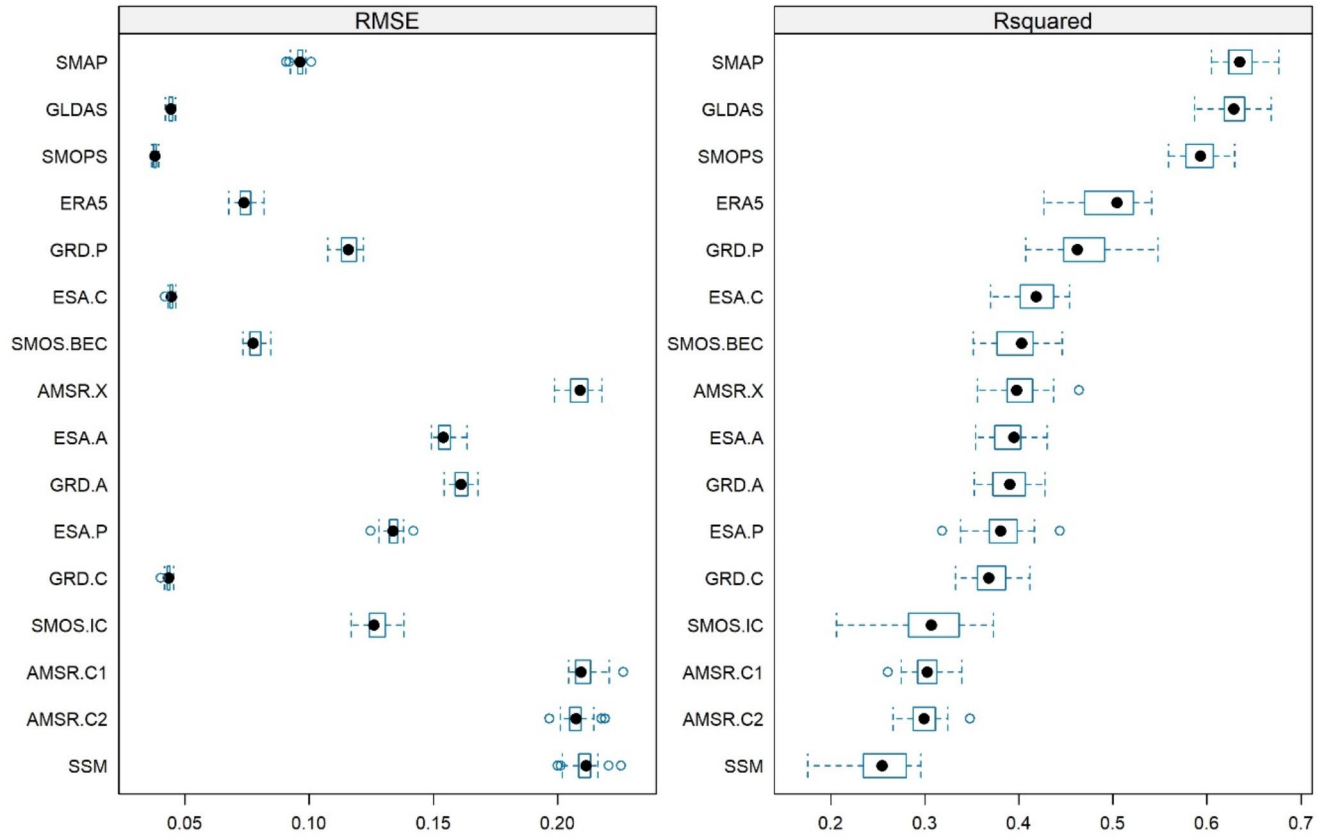

Fig. 7 Comparison of RMSE and R^2 values in perspective of the datasets

Most favorable errVars belonged to ERA5, GLDAS, SMOPS, and GRD.C SM products, having the lowest values with the smallest IQRs, indicating the stability of the given product against all others (Fig. 10).

For rho2s, all strong correlations had large IQRs, indicating that SM products had varying relations in the triplets of the ETC analysis. GRD.P had the largest correlations, with a median of 0.64, followed by the GRD.A with a median of 0.51. SMOPS's median was slightly smaller (rho2 = 0.47). Rho2 was 0.34 for SMAP, meaning 0.58 as a correlation coefficient, but it is still relevant among the SM products (Fig. 11).

Considering both ETC measures, the largest Mean_rho2 and lowest Mean_errVar indicated superior performance, and there were discrepancies, i.e., rank was different by the two metrics: GRD.P, GRD.C, and SMOPS can be considered the best, while SMAP and ERA5, although having low Mean_errVar, had lower Mean_rho2 values (Fig. 9), were still in the acceptable range.

We compared the ETC and the model-based metrics and the largest discrepancies were observed for GLDAS and GRD.A data. While GLDAS generally performed well in the model-based accuracy metrics, its performance was only considered acceptable based on the Mean_errVar metric in the ETC analysis. Additionally, GRD.A fell into the low-performance cluster of the model-based evaluation and had the second highest Mean_rho2 and highest Mean_errVar.

Furthermore, we quantified the correlations among the ETC and model-based metrics (Fig. 12). Mean error variances (errVar) had strong correlations with the RMSE (0.90), ubRMSE (0.90), wR2 (-0.75), UMAP dimension (0.73), NSE (-0.66), and moderate relationship with the KGE (-0.54). The standard error of the errVar was in strong correlation with the RMSE and ubRMSE (0.76), and the UMAP dimensions (0.66 and 0.60).

3.7 Key Environmental Factors of the Models

During the modeling phase, the order of input environmental factors and their corresponding median values for R^2 (Table 2) were determined for each SM product. The selection of environmental factors for each model was determined based on the results of 16 models. Both precipitation (sum of one day) and maximum temperature (sum for the preceding seven days) were included in the predictors in each model, being selected 16 times out of 16 models. The Köppen-Geiger class was also a primary factor in 15 out of 16 cases. Additionally, the MODIS NDVI index and

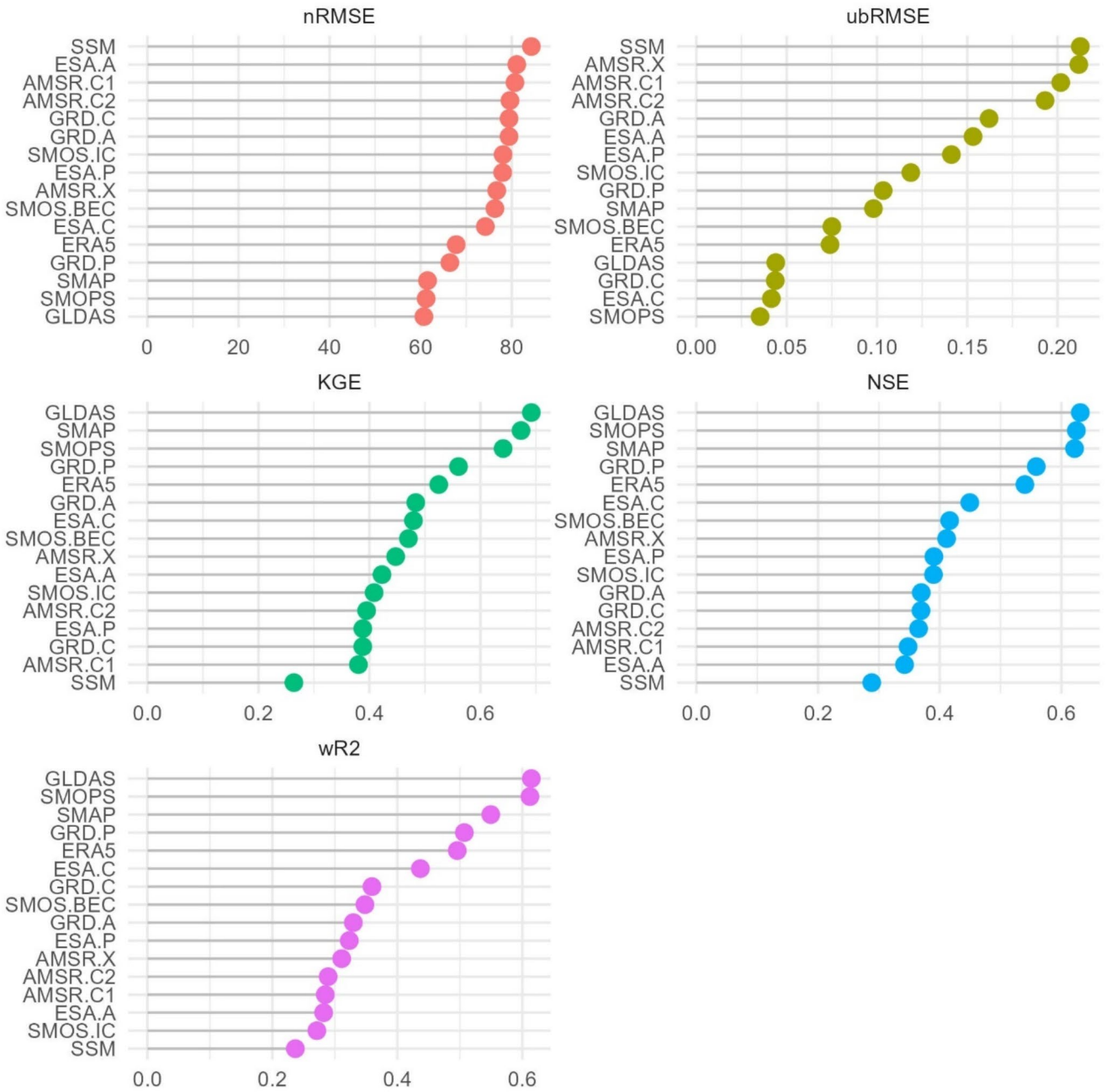

Fig. 8 nRMSE (%), ubRMSE (m^3/m^3), KGE, NSE and wR^2 values of SM products

topographic categories (i.e., EUDEM.CODE) were frequently selected predictors, being selected in 12 out of 16 and 11 out of 16 models, respectively. Additionally, factors related to field water capacity, soil texture, and certain DEM-derived topographic factors were present with varying levels of importance.

4 Discussion

4.1 Differences of SM Data by Satellite Products

We found that the highest IQR of SMs (0.41–0.78 m^3/m^3) belonged to AMSR.X and AMSR.C2 except in one case where the GRD.A had the highest IQR. Conversely, the smallest IQRs (0–0.04 m^3/m^3) were observed for SSM, GRD.P, SMOS.IC, SMOS.BEC, GRD.C and SMOPS. The standard deviation between the medians within each

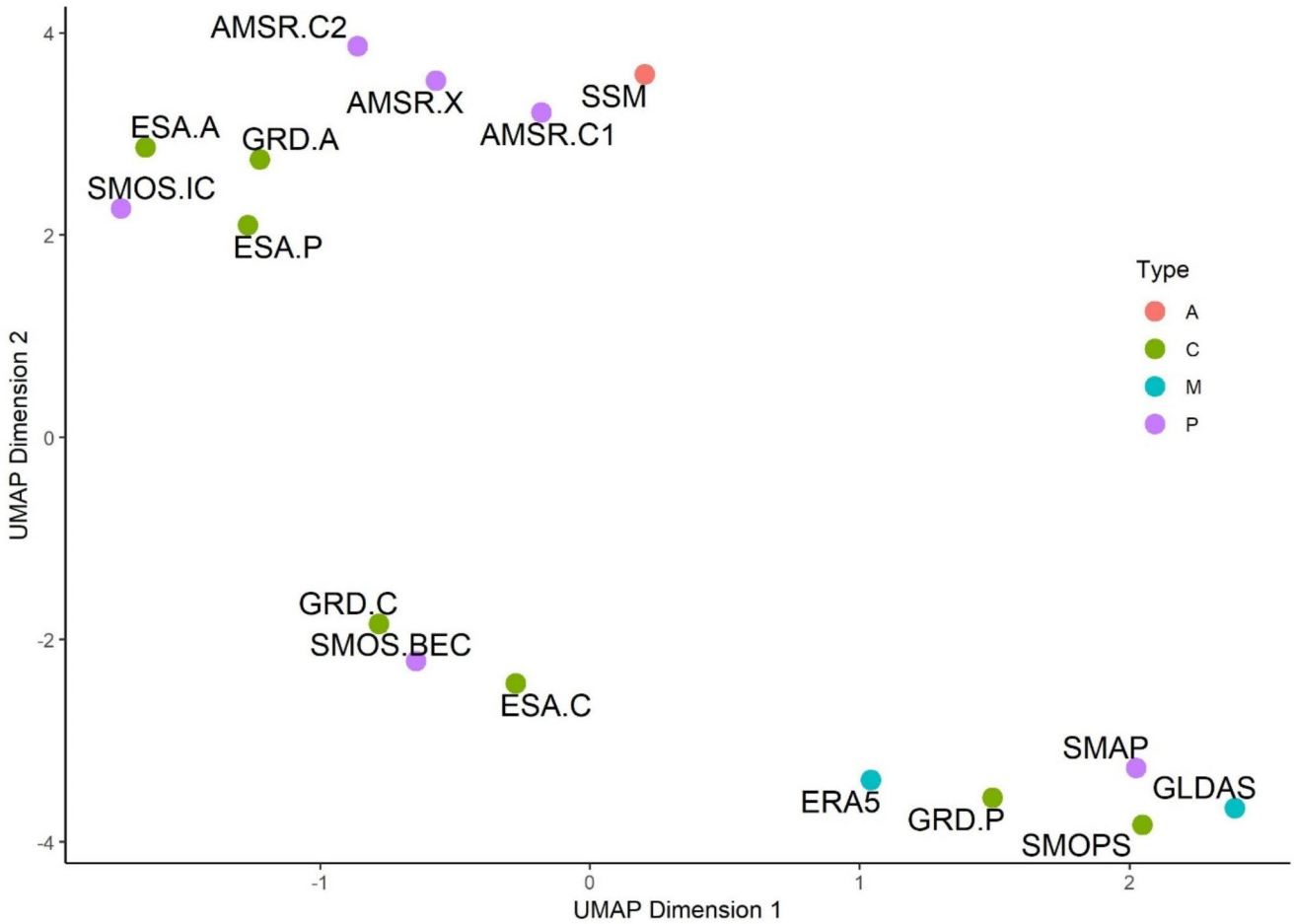

Fig. 9 Accuracy pattern of soil moisture data based on UMAP dimension reduction (A: active, P: passive, C: combined, M: modelled type of products)

group was most pronounced for high mountains and zone B (0.181), and D (0.211). Meanwhile, the smallest standard deviation in medians was observed for zone C in plains (0.066) and hills (0.082) (Table 1). We found that the elements of the high mountain category, climate zone B and E differed, this is because only 73 belonged to climate zone B, 47 to climate zone E, and 24 to the high mountain category from the 1454 sample points. However, these regions covered a relevantly smaller area compared to climate zones C and D at the European level (Fig. 4). In this study, category B covers 5% and category E 3% in Europe, while category C covers 39% and category D 53%.

In terms of correlation (Fig. 5), the result called the attention of dissimilarities, i.e., at the same location and same date, different SM products had different values, and the relationship among the different datasets cannot be described with linear or non-linear functions. This gives a special relevance on finding the most reliable data sources, as these data are used in regional planning or used as input data in predictive models (climate change, irrigation, etc.). The best correlations were obtained for ESA.P and GRD.P, ESA.C and GRD.C. This result can be attributed to the substantial similarity between the ESA and GRD datasets, with the distinction that ESA also incorporates GMI, MWRI data, while GRD uses GLWD, GTOPO30, ISMN data (Dorigo et al. 2021b; Scanlon et al. 2021). Ray et al. (2017) investigated the dry and wet days using the data of SMOS (from Barcelona Expert Centre), AMSR2, and SMAP, and found that over the period 2010–2016, the correlation of SMOS-SMAP ranged from 0.66 to 0.91, SMOS-AMSR2 from 0.10 to 0.59, and SMAP-AMSR2 from 0.1 to 0.8 for the studied points. In contrast, in the present study, SMOS.BEC-SMAP ranged 0.38, SMOS.BEC-AMSR between 0.27 and 0.33, and SMAP-AMSR between 0.34 and 0.45. The differences can be explained by the specific regional characteristics: our study four climate zones in Europe (spanning from the Mediterranean to polar regions) and four topographic regions (ranging from plains to high mountains), which pointed on the relevance of the given area: the correlation structure relevantly differed by the climatic zones based on

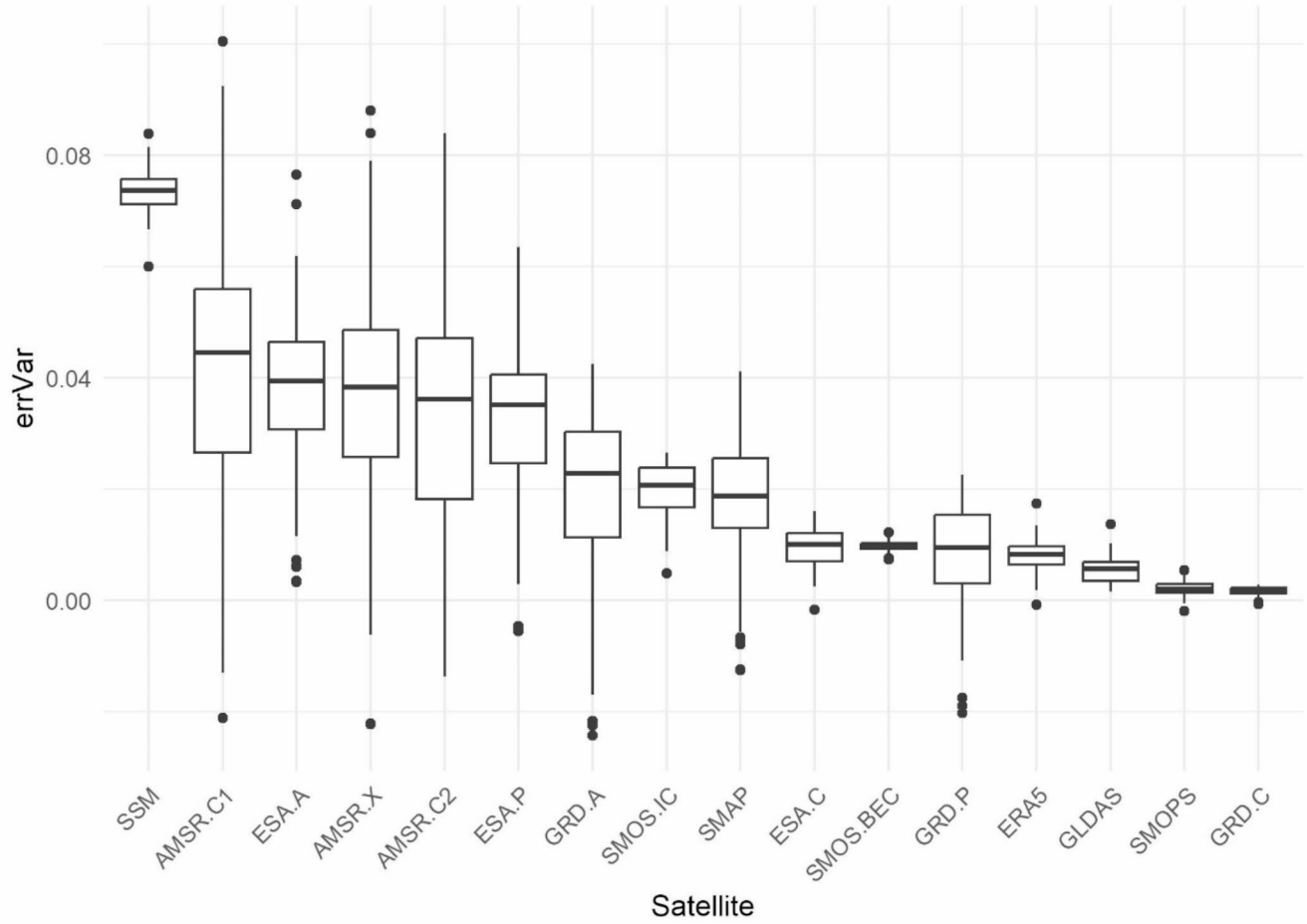

Fig. 10 Distribution of error variances (errVar) by satellites

the Mantel test. In arid areas the SM products had stronger correlations, which can be the consequence of dry soils, i.e., if the whole area is dry, the biasing factors' influence is also smaller, consequently, the patterns are similar. However, in temperate and continental zones there can be spatial differences, and the drought is not completely true due to local rainfalls, varying evaporation and the vegetation is also spatially different. Ray et al. (2017) conducted their analysis in Texas in a less variable dry environment, which justifies our hypothesis. (Fan et al. 2025) demonstrated that SM retrieval accuracy varies significantly across land cover types, with optimal performance in croplands, grasslands, and cropland/natural vegetation mosaics, while noting substantial estimation errors in areas characterized by complex topography, such as steep slopes, forests, and desert regions, where surface properties substantially affect backscatter signal interpretation. The high mountains with their special climate represented a unique environment, but their differing correlation (see Mantel test results) is also the consequence of the lesser spatial extent and data.

4.2 Efficacy Issues of Modeling and Error Variance

In the context of statistical modeling, where satellite products serve as target variable, it was determined that RF models for GLDAS and SMOPS exhibited the lowest RMSE and the highest R^2 (Fig. 6): GLDAS (RMSE: 0.044 m^3/m^3; R^2: 0.628) and SMOPS (RMSE: 0.037 m^3/m^3; R^2: 0.592). Accordingly, these two data products may provide estimates closest to real SM states, with environmental factors accounting for the most variance in these cases. Conversely, the largest RMSE errors were obtained for the AMSR models (0.208–0.209 m^3/m^3) and SSM (0.211 m^3/m^3). The smallest R^2 values were associated with the SSM (0.254) and AMSR.C2 (0.299) indicating increased model inaccuracy and a poor explanation of environmental variable variance in these instances. We examined the relationship between the observed values and the modelled values. This led us to conclude that SMOPS (nRMSE:61.2, ubRMSE:0.03, KGE:0.640, NSE:0.624, wR^2: 0.612) and GLDAS (nRMSE:60.7, ubRMSE:0.04, KGE:0.691, NSE:0.631, wR^2: 0.614) gave the best results (Fig. 8).

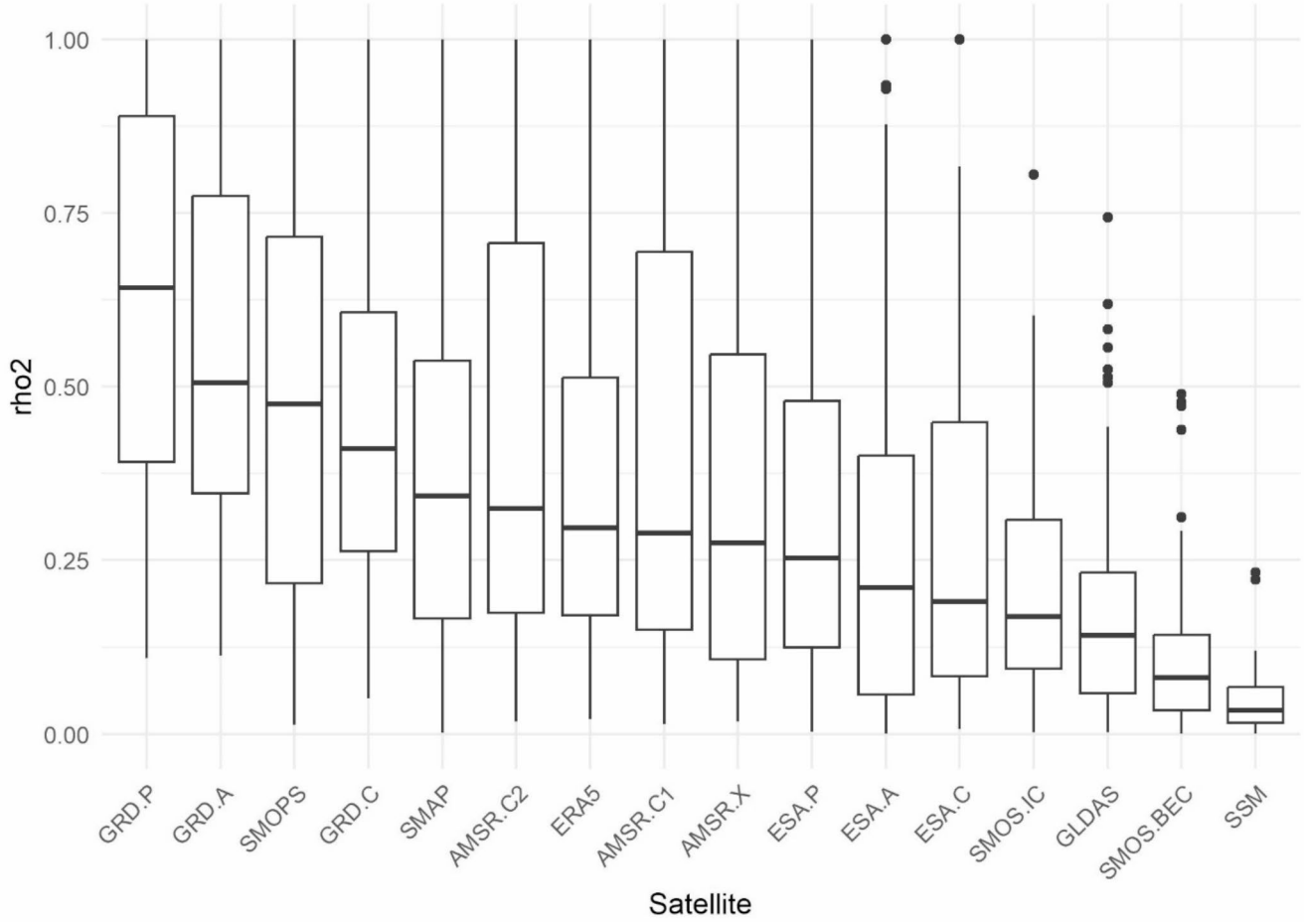

Fig. 11 Distribution of the rho2s by satellites

The primary variables chosen for the models were primarily weather and climate-related factors, such as precipitation, maximum temperature, and Köppen climatic zone, as well as topography categories (Supplement 2). Soil texture was the seventh most frequent variable in the models. According to Gibon et al. (2024), land cover, topography categories, and soil properties (texture, organic matter) had significant effects on the SMOS's uncertainty, which is consistent with our general findings regarding the key factors affecting accuracy in modeling. However, our experiment revealed that NDVI alone did not make a significant contribution to the models. The influence of vegetation on SM data did not identify consistent linear relationship with the MODIS NDVI values (Fig. 13), the R^2 values did not explain large variance.

Bhardwaj et al. (2022) examined the AMSR2, SMOS, SMAP, and SMOPS data with TCA, supplemented with modelled data such as ERA5-Land and GLDAS, and in-situ data (OzNet, CosmOz, OzFlux). They concluded that SMOS (from Barcelona Expert Centre) provided the best results but ASMR2 and SMAP showed outliers for Australia and the South-West Pacific: compared to the values of the individual stations, the RMSE values for SMOS were less than 0.1, while SMOPS, AMSR2 and SMAP went above 0.1. Kugler et al. (2024) found that SMAP overperformed SMOS in a linear analysis of river flow monitoring, and Gibon et al. (2024) pointed to possible sources of uncertainties of SMOS data on a global scale highlighting the role of terrain and soil properties. This result aligns with our study, with their respective RMSE values: SMOS.BEC exhibited an RMSE of 0.08, SMOPS with 0.04, and SMAP performed well with an RMSE of 0.10. In contrast, the AMSR models, when considering environmental factors, yielded higher RMSE values ranging from 0.19 to 0.21. Zheng et al. (2022) analyzed 24 different satellite SM datasets (of which ERA5-Land, ESA, GLDAS, SMOS (from INRA-CESBIO) and AMSR2 were included in our study) and compared them based on the SMN-SDR network data in the Shandian River Basin, China, using TCA. According to their findings, ESA.C showed the best results, with an RMSE of 0.028, ESA.P 0.063, and ESA.A 0.073, while GLDAS 0.038, ERA5-Land ranged from 0.076 to 0.080, SMOS ranged from 0.111 to 0.118 and AMSR2 RMSE ranged from 0.063 to 0.103. In our case, the ESA showed a moderately good result, RMSE

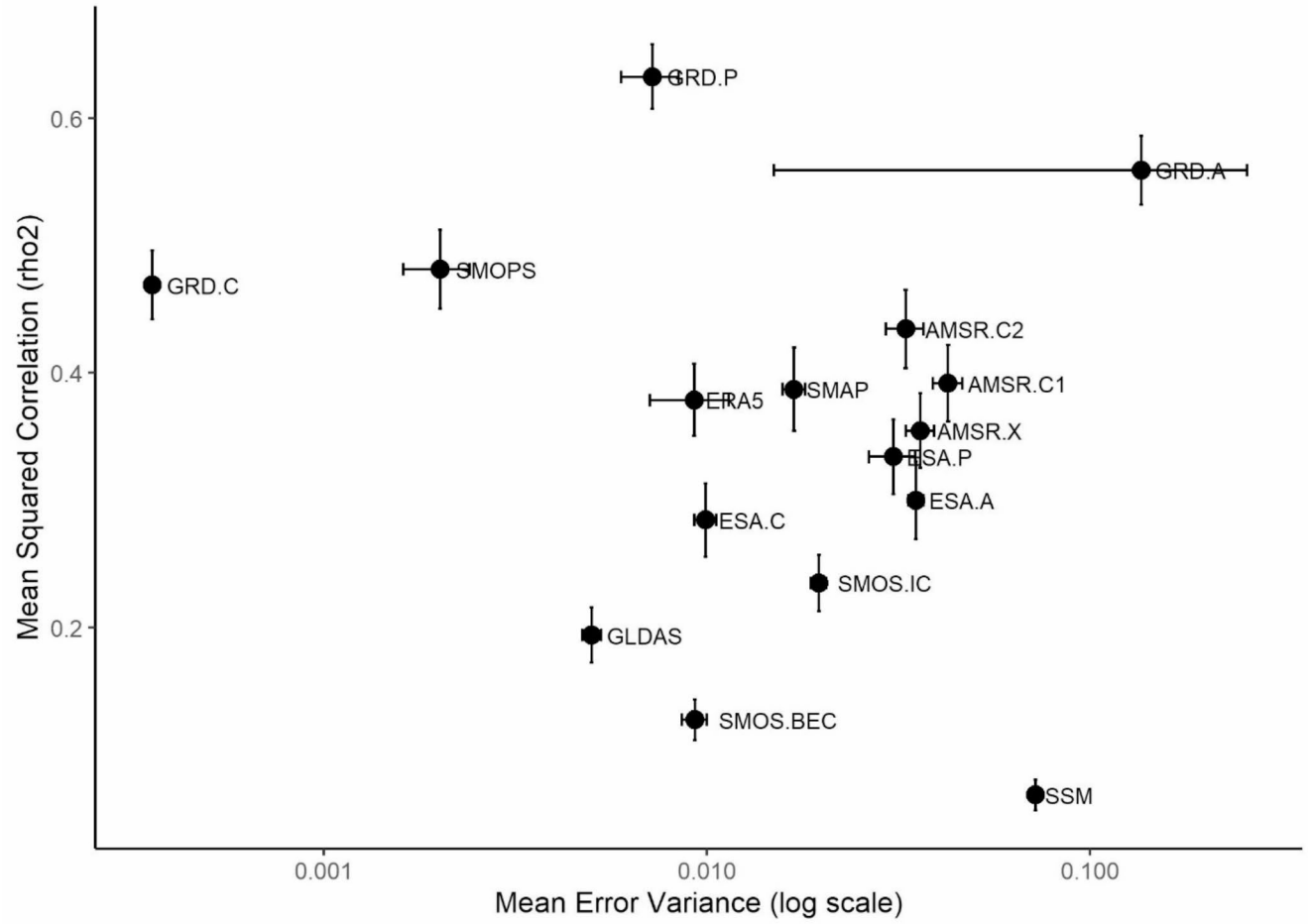

Fig. 12 Pattern of the soil moisture data based on the Extended Triple Collocation Analysis (whiskers: ±1 × standard error)

values as follows: ESA.C 0.04, ESA.P 0.14, ESA.A 0.15, and AMSR2 ranged from 0.19 to 0.21. The current RMSE value of GLDAS 0.04, ERA5 0.07, and SMOS.IC 0.12 more closely with the findings of Zheng et al. (2022). In a global investigation by Ma et al. (2019), which considered various products including AMSR2, ESA CCI, SMAP, and SMOS-IC across different climatic regions and accounting for confounding factors using ISMN data, the average ubRMSE for AMSR was 0.143, for ESA it was 0.041, SMAP it was 0.043 and for SMOS-IC it was 0.048. In our study, AMSR exhibited values ranging between 0.19 and 0.21, while ESA were found between 0.04 and 0.15, SMAP was 0.10, and SMOS. IC was 0.12. Mazzariello et al. (2023) conducted an evaluation, including the assessment of ESA, SSM, and SMOS-IC models for Europe, considering ecoregions and incorporating factors such as geographical heterogeneity, climate, and land cover. The study compared these models with measurements from the ISMN in-situ network. Their findings indicated that ESA demonstrated favorable results, while SSM showed the lowest performance. Specifically, for ubRMSE, ESA values were below 0.10 for each ecoregion and SSM and SMOS-IC were below 0.20. In our study, the ESA models ranged between 0.04 and 0.15, while the SSM model was 0.21 and SMOS.IC was 0.12.

The evaluation of model-based metrics using UMAP dimension reduction and ETC provided insights into patterns and clusters of similar products. While these approaches differed significantly in their calculation methods, they yielded comparable outputs with some notable distinctions. GLDAS performed exceptionally well in the model-based evaluation, achieving the highest NSE, KGE, and wR2 scores, along with low nRMSE and ubRMSE values. However, it demonstrated weaker performance according to ETC, with low Mean_rho2 and Mean_errVar scores. This discrepancy suggests that although GLDAS was highly predictable using environmental factors in the model, ETC revealed that only 20% of its values could be attributed to the true signal. The low Mean_errVar indicated consistent values and minimal random error. Another notable difference between the two evaluations was observed in GRD.A. Based on model-based accuracy metrics; this product ranked in the middle to lower range among the 16 products evaluated. This ranking may

Table 2 Summary of model accuracies and most important predictors (selected by the recursive feature Elimination)

SM Data	AMSR.C1	AMSR.C2	AMSR.X	ERA5	ESA.A	ESA.C	ESA.*P*	GLDAS
R^2(median)	0.30	0.29	0.39	0.50	0.39	0.41	0.38	0.62
Variables (decreasing importance)	1. MODIS.NDVI 2. T.MAX.SUM.7 3. EUDEM.CODE 4. PREC.S.1 5. WATER.C.FC.05 6. SOIL.TEX.05 7. KÖPPEN 8. TPI	1. MODIS.NDVI 2. T.MAX.SUM.7 3. SOIL.TEX.05 4. PREC.S.1 5. EUDEM.CODE 6. KÖPPEN 7. CROSS.S.C 8. WATER.C.FC.05	1. MODIS.NDVI 2. T.MAX.SUM.7 3. PREC.S.1 4. KÖPPEN 5. MRRTF 6. EUDEM.CODE 7. WATER.C.FC.05 8. TPI	1. T.MAX.SUM.7 2. PREC.S.1 3. KÖPPEN 4. SAND.M.05 5. CLAY.M.05 6. MODIS.NDVI 7. MRRTF 8. MRVBF 9. WATER.C.FC.05 10. CONV.I 11. MAX.C 12. EUDEM.CODE 13. CROSS.S.C 14. MIN.C 15. PLAN.C 16. LONGIT.C 17. SOIL.TEX.05 18. PROF.C 19. TPI	1. PREC.S.1 2. KÖPPEN 3. T.MAX.SUM.7 4. EUDEM.CODE 5. MODIS.NDVI 6. MRRTF	1. KÖPPEN 2.T.MAX.SUM.7 3. MODIS.NDVI 4. PREC.S.1 5. MRRTF	1. KÖPPEN 2. T.MAX.SUM.7 3. MODIS.NDVI 4. PREC.S.1 5. WATER.C.FC.05	1. MODIS.NDVI 2. T.MAX.SUM.7 3. KÖPPEN 4. WATER.C.FC.05 5. EUDEM.CODE 6. SOIL.TEX.05 7. PREC.S.1 8. MRVBF

SM Data	**GRD.A**	**GRD.C**	**GRD.P**	**SMAP**	**SMOPS**	**SMOS.BEC**	**SMOS.IC**	**SSM**
R^2(median)	0.39	0.36	0.46	0.63	0.59	0.40	0.30	0.25
Variables (decreasing importance)	1. KÖPPEN 2. WATER.C.FC.05 3. PREC.S.1 4. T.MAX.SUM.7 5. SOIL.TEX.05	1. KÖPPEN 2. WATER.C.FC.05 3. PREC.S.1 4. T.MAX.SUM.7 5. SOIL.TEX.05 6. PROF.C	1. KÖPPEN 2. WATER.C.FC.05 3. T.MAX.SUM.7 4. MRVBF 5. PREC.S.1 6. MIN.C 7. EUDEM.CODE 8. SOIL.TEX.05 9. LONGIT.C 10. TPI 11. CONV.I 12. PROF.C 13. MRRTF 14. CROSS.S.C	1. T.MAX.SUM.7 2. PREC.S.1 3. KÖPPEN 4. WATER.C.FC.05 5. EUDEM.CODE 6. MODIS.NDVI 7. MRVBF	1. T.MAX.SUM.7 2. MODIS.NDVI 3. WATER.C.FC.05 4. KÖPPEN 5. PREC.S.1 6. SOIL.TEX.05 7. MRVBF 8. EUDEM.CODE 9. MRRTF	1. T.MAX.SUM.7 2. KÖPPEN 3. WATER.C.FC.05 4. MODIS.NDVI 5. PREC.S.1 6. SOIL.TEX.05 7. EUDEM.CODE 8. MRVBF 9. TPI 10. MRRTF	1. T.MAX.SUM.7 2. CLAY.M.05 3. SAND.M.05 4. WATER.C.FC.05 5. MRVBF 6. MRRTF 7. MIN.C 8. MODIS.NDVI 9. PREC.S.1 10. CONV.I 11. EUDEM.CODE 12. LONGIT.C 13. KÖPPEN 14. PROF.C 15. SOIL.TEX.05 16. CROSS.S.C 17. MAX.C 18. PLAN.C 19. TPI	1. PREC.S.1 2. T.MAX.SUM.7

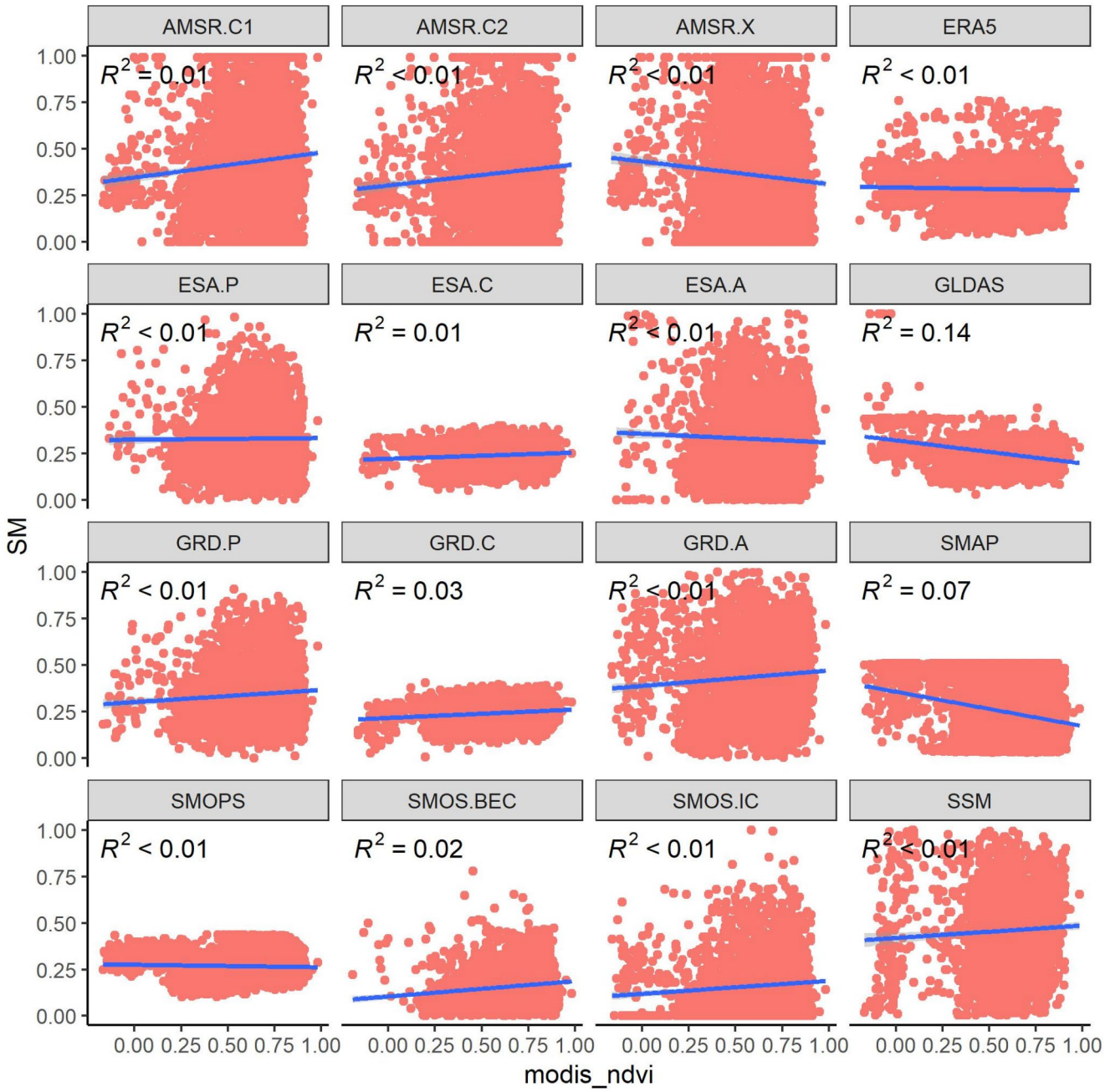

Fig. 13 The scatterplot of Modis NDVI and SM values

be associated with its highest Mean_errVar (0.14), indicating significant random variability and low precision. However, its high Mean_rho2 (0.57) suggested that the values of this product more accurately reflected the true value, exhibiting a low signal-to-noise ratio (McColl et al. 2014). Despite these differences, the evaluation methods revealed similar patterns. GRD.P, SMOPS, and SMAP consistently emerged as the best-performing products across both evaluation approaches. The accuracy and unbiased nature of SMAP were also reported by Chen et al. (2017). GRD.A was an outlier in several terms: it was the only SM product with high rho2 and the lowest errVar, while the RMSE was high. Overall, UMAP dimensions exhibited strong correlations with Mean_errVar (Spearman's r: 0.72 and 0.73 for UMAP dimensions 1 and 2, respectively). However, no significant relationship was observed with Mean_rho2 (-0.16 and −0.15). This suggests that the accuracy metrics of models constructed using environmental factors are primarily associated with consistency or random error but fail to account for the fraction of true signal variance. The date

of the SM products was considered only in 3 months; thus, we focused on the spatial rather than the temporal aspects. (Brocca et al. 2024) computed monthly averages of SM, and found that the SM products (ASCAT, ESA.CCI, SMAP, S1-RT1, S1-COP) had high temporal consistency. Generally, the SM products' reliability is better in time than in space, which should be considered when involved in different models.

4.3 Limitations

In the studies used in the discussion, SM frequently relied on data from in-situ networks such as ISMN (Ma et al. 2019; Gruber et al. 2020; Mazzariello et al. 2023), OzNet, CosmOz, OzFlux (Bhardwaj et al. 2022), SMN-SDR (Zheng et al. 2022). These networks are often regional and may lack the necessary density to be representative of the entire European region, considering its diverse climate and topography. In contrast, our study utilized 1454 spatially evenly distributed sampling points, providing a comprehensive portrayal of 16 SM data products across Europe in terms of both climate and topography. It is essential to acknowledge that the data used in our study faced challenges such as satellite pass-induced gaps, particularly notable in the case of SSM. The varied resolution of the data (ranging from 1 to 25 km) and the presence of dense vegetation in European areas also influenced the obtained SM results.

Furthermore, limitations in SM analysis were identified in snow-covered, frozen areas, and high mountain areas, particularly in the E Köppen zone and the high mountain category. In addition, the presence of small water bodies may introduce modifications to values at individual sampling points.

5 Conclusions

We aimed to compare the SM data of 16 satellite-based SM products throughout three seasons, climatic zones, and topography; furthermore, we hypothesized (i) that environmental factors should be good predictors of the SM in a statistical modeling scheme, and that (ii) error variance of ETC and accuracy metrics of the models are correlating. We found that SM products provided different values exhibiting variations across data sources (i.e. satellites) and had relevant differences in all combinations of climate and topography. Correlations among SM products were usually low ($r<0.5$), the closest relationships were found between ESA.P and GRD.P, ESA.C and GRD.C, while the lowest values were for GLDAS. Based on the models including environmental factors, we found that GLDAS and SMOPS produced the lowest RMSE and the highest R^2 values; thus, these two models best reflected the individual environmental factors. Based on the relationship between the observed and the modelled values, the SMOPS and GLDAS provided the best results, while the SSM had the least good results. The multivariate evaluation using the UMAP technique and the ETC demonstrated enhanced reliability, characterized by reduced uncertainty, for both SMOPS and GLDAS. A strong correlation ($r=0.73$; $p<0.001$) was observed between UMAP dimensions and the Mean_errVar of ETC. The SMOPS soil moisture product exhibited superior performance in modeling environmental factors and yielded the lowest error variance in the Triple Collocation Analysis (TCA). Furthermore, GRD.P emerged as the most reliable product based on ETC results, despite ranking fourth in both NSE and KGE metrics but within the best-performing cluster defined by UMAP. However, as there is no absolute reference data, it is not easy to name one SM product: if the requirement is the highest rho2, the GRD.P is the best product, regarding the errVar, the GRD.C, and SMOPS can be a good option followed by the GRD.P, and if we rely on the SM reflected by the environmental factors, the GLDAS, SMOPS, SMAP, and GRD.P seems the best choice. The intersection of the different approaches can be the GRD.P and the SMOPS. This analysis calls attention to the differences, and potential errors when these SM data sources are involved in planning.

Supplementary Information The online version contains supplementary material available at https://doi.org/10.1007/s41748-025-00605-2.

Acknowledgements The project was funded by the NKFI K138079 and the framework of the Széchenyi Plan Plus program with the support of the RRF 2.3.1 21 2022 00008 project.

Funding Open access funding provided by University of Debrecen.

Declarations

Conflict of interest The authors declare that they have no known competing financial interests or personal relationships that could have appeared to influence the work reported in this paper.

References

Albergel C, de Rosnay P, Balsamo G et al (2012) Soil moisture analyses at ECMWF: evaluation using global Ground-Based in situ observations. J Hydrometeorol 13:1442–1460. https://doi.org/10.1175/JHM-D-11-0107.1

Ambrosone M, Matese A, Di Gennaro SF et al (2020) Retrieving soil moisture in rainfed and irrigated fields using Sentinel-2 observations and a modified OPTRAM approach. Int J Appl Earth Obs Geoinf 89:102113. https://doi.org/10.1016/j.jag.2020.102113

Babaeian E, Sadeghi M, Franz TE et al (2018) Mapping soil moisture with the optical trapezoid model (OPTRAM) based on long-term MODIS observations. Remote Sens Environ 211:425–440. https://doi.org/10.1016/j.rse.2018.04.029

Bakker JD (2024) Applied multivariate statistics in R. University of Washington

Bauer-Marschallinger B (2018) Copernicus global land operations vegetation and energy. Validation Rep Surface soil moisture collection 1km(Version 1):Issuei120

Bauer-Marschallinger B (2019) Copernicus Global Land Operations Vegetation and Energy. Product user manual. Surface soil moisture Collection 1km Version 1. Issue I1.30

Bauer-Marschallinger B, Cao S, Schaufler S et al (2017) 1km Soil Moisture from Downsampled Sentinel-1 SAR Data: Harnessing Assets and Overcoming Obstacles. 17330

Bauer-Marschallinger B, Paulik C, Hochstöger S et al (2018) Soil moisture from fusion of scatterometer and SAR: closing the scale gap with Temporal filtering. Remote Sens 10:1030. https://doi.org/10.3390/rs10071030

Bauer-Marschallinger B, Freeman V, Cao S et al (2019) Toward global soil moisture monitoring with Sentinel-1: Harnessing assets and overcoming Obstacles. IEEE Trans Geosci Remote Sens 57:520–539. https://doi.org/10.1109/TGRS.2018.2858004

Beck HE, Pan M, Miralles DG et al (2021) Evaluation of 18 satellite- and model-based soil moisture products using in situ measurements from 826 sensors. Hydrol Earth Syst Sci 25:17–40. https://doi.org/10.5194/hess-25-17-2021

Bertalan L, Holb I, Pataki A et al (2022) UAV-based multispectral and thermal cameras to predict soil water content – A machine learning approach. Comput Electron Agric 200:107262. https://doi.org/10.1016/j.compag.2022.107262

Bhardwaj J, Kuleshov Y, Chua Z-W et al (2022) Evaluating satellite soil moisture datasets for drought monitoring in Australia and the South-West Pacific. Remote Sens 14:3971. https://doi.org/10.3390/rs14163971

Blanka-Végi V, Tobak Z, Sipos G et al (2025) Estimation of the Spatio-temporal variability of surface soil moisture using machine learning methods integrating satellite and Ground-based soil moisture and environmental data. https://doi.org/10.1007/s11269-024-04069-3. Water Resour Manage

Brocca L, Gaona J, Bavera D et al (2024) Exploring the actual Spatial resolution of 1 Km satellite soil moisture products. Sci Total Environ 945:174087. https://doi.org/10.1016/j.scitotenv.2024.174087

Calvet J-C, Fritz N, Froissard F et al (2007) In situ soil moisture observations for the CAL/VAL of SMOS: the SMOSMANIA network. In: 2007 IEEE International Geoscience and Remote Sensing Symposium. IEEE, Barcelona, Spain, pp 1196–1199

Chai T, Draxler RR (2014) Root mean square error (RMSE) or mean absolute error (MAE)? – Arguments against avoiding RMSE in the literature. Geosci Model Dev 7:1247–1250. https://doi.org/10.5194/gmd-7-1247-2014

Chen X, Hu Q (2004) Groundwater influences on soil moisture and surface evaporation. J Hydrol 297:285–300. https://doi.org/10.1016/j.jhydrol.2004.04.019

Chen Y, Yang K, Qin J et al (2013) Evaluation of AMSR-E retrievals and GLDAS simulations against observations of a soil moisture network on the central Tibetan plateau: EVALUATE SOIL MOISTURE PRODUCTS ON TIBET. J Geophys Res Atmos 118:4466–4475. https://doi.org/10.1002/jgrd.50301

Chen F, Crow WT, Colliander A et al (2017) Application of triple collocation in Ground-Based validation of soil moisture active/passive (SMAP) level 2 data products. IEEE J Sel Top Appl Earth Observations Remote Sens 10:489–502. https://doi.org/10.1109/JSTARS.2016.2569998

Colliander A, Jackson TJ, Bindlish R et al (2017) Validation of SMAP surface soil moisture products with core validation sites. Remote Sens Environ 191:215–231. https://doi.org/10.1016/j.rse.2017.01.021

Colliander A, Reichle RH, Crow WT et al (2022) IEEE J Sel Top Appl Earth Observations Remote Sens 15:364–392. https://doi.org/10.1109/JSTARS.2021.3124743. Validation of Soil Moisture Data Products From the NASA SMAP Mission

Copernicus Climate Change Service (2019) ERA5-Land monthly averaged data from 1950 to present

Crow WT, Wagner W, Naeimi V (2010) The impact of radar incidence angle on Soil-Moisture-Retrieval skill. IEEE Geosci Remote Sens Lett 7:501–505. https://doi.org/10.1109/LGRS.2010.2040134

Dai A (2011) Drought under global warming: a review. WIREs Clim Change 2:45–65. https://doi.org/10.1002/wcc.81

Diouf D, Mejia C, Seck D (2020) Soil Moisture Prediction Model from ERA5-Land Parameters using a Deep Neural Networks: In: Proceedings of the 12th International Joint Conference on Computational Intelligence. SCITEPRESS - Science and Technology Publications, Budapest, Hungary, pp 389–395

Dobriyal P, Qureshi A, Badola R, Hussain SA (2012) A review of the methods available for estimating soil moisture and its implications for water resource management. J Hydrol 458–459:110–117. https://doi.org/10.1016/j.jhydrol.2012.06.021

Dorigo WA, Gruber A, De Jeu RAM et al (2015) Evaluation of the ESA CCI soil moisture product using ground-based observations. Remote Sens Environ 162:380–395. https://doi.org/10.1016/j.rse.2014.07.023

Dorigo W, Himmelbauer I, Aberer D et al (2021a) The international soil moisture network: serving Earth system science for over a decade. Hydrol Earth Syst Sci 25:5749–5804. https://doi.org/10.5194/hess-25-5749-2021

Dorigo W, Scanlon T, Buttinger P et al (2021b) Product User Guide and Specification. Land Service: Soil Moisture ECV. D3.SM.5-v3.0

Dorigo W, Scanlon T, Preimesberger W, Kidd R (2021c) Product Quality Assessment Report. Land Service: Soil Moisture ECV D2.SM.2-v3.0

Doubkova M, Wagner W, Naeimi V et al (2016) The Use of Sentinel-1 for Monitoring of Soil Moisture within the Copernicus Global Land Service. 740:105

Du Y, Ulaby FT, Dobson MC (2000) Sensitivity to soil moisture by active and passive microwave sensors. IEEE Trans Geosci Remote Sens 38:105–114. https://doi.org/10.1109/36.823905

Dunn PK, Smyth GK (2018) Generalized linear models with examples in R. Springer New York, New York, NY

Entekhabi D, Rodriguez-Iturbe I, Castelli F (1996) Mutual interaction of soil moisture state and atmospheric processes. J Hydrol 184:3–17. https://doi.org/10.1016/0022-1694(95)02965-6

Fan D, Zhao T, Jiang X et al (2025) A Sentinel-1 SAR-based global 1-km resolution soil moisture data product: algorithm and preliminary assessment. Remote Sens Environ 318:114579. https://doi.org/10.1016/j.rse.2024.114579

Fernandez-Moran R, Wigneron J-P, De Lannoy G et al (2017) A new calibration of the effective scattering albedo and soil roughness parameters in the SMOS SM retrieval algorithm. Int J Appl Earth Obs Geoinf 62:27–38. https://doi.org/10.1016/j.jag.2017.05.013

Field A (2013) Discovering statistics with IBM SPSS statistics. Sage, Newbury Park, CA

Fischer EM, Seneviratne SI, Vidale PL et al (2007) Soil Moisture–Atmosphere interactions during the 2003 European summer heat wave. J Clim 20:5081–5099. https://doi.org/10.1175/JCLI4288.1

Ford TW, Quiring SM (2019) Comparison of contemporary in situ, model, and satellite remote sensing soil moisture with a focus on drought monitoring. Water Resour Res 55:1565–1582. https://doi.org/10.1029/2018WR024039

Forkuor G, Hounkpatin OKL, Welp G, Thiel M (2017) High resolution mapping of soil properties using remote sensing variables in South-Western Burkina Faso: A comparison of machine learning and multiple linear regression models. PLoS ONE 12:e0170478. https://doi.org/10.1371/journal.pone.0170478

Fung A, Eom H (1985) A comparison between active and passive sensing of soil moisture from vegetated terrains. IEEE Trans Geosci Remote Sens GE –23:768–775. https://doi.org/10.1109/TGRS.1985.289396

Garg A, Munoth P, Goyal R (2016) Application of soil moisture sensor in agriculture. In Proceedings of Internation Conference on Hydraulic (pp. 8–10)

GCOS-138 (2010) Implementation plan for the global observing system for climate in support of the unfccc (2010 update)

Ghasemloo N, Matkan AA, Alimohammadi A et al (2022) Estimating the agricultural farm soil moisture using spectral indices of Landsat 8, and Sentinel-1, and artificial neural networks. J Geovis Spat Anal 6:19. https://doi.org/10.1007/s41651-022-00110-4

Gibon F, Mialon A, Richaume P et al (2024) Estimating the uncertainties of satellite derived soil moisture at global scale. Sci Remote Sens 10:100147. https://doi.org/10.1016/j.srs.2024.100147

Gruber A, Scanlon T, van der Schalie R et al (2019) Evolution of the ESA CCI soil moisture climate data records and their underlying merging methodology. Earth Syst Sci Data 11:717–739. https://doi.org/10.5194/essd-11-717-2019

Gruber A, De Lannoy G, Albergel C et al (2020) Validation practices for satellite soil moisture retrievals: what are (the). errors? Remote Sens Environ 244:111806. https://doi.org/10.1016/j.rse.2020.111806

Hanson BR, Orloff S, Peters D (2000) Monitoring soil moisture helps refine irrigation management. Cal Ag 54:38–42. https://doi.org/10.3733/ca.v054n03p38

Heathman GC, Starks PJ, Ahuja LR, Jackson TJ (2003) Assimilation of surface soil moisture to estimate profile soil water content. J Hydrol 279:1–17. https://doi.org/10.1016/S0022-1694(03)00088-X

Hirschi M, Nicolai-Shaw N, Preimesberger W et al (2021) ESA climate change initiative Plus - Soil moisture. Algorithm theoretical baseline document (ATBD) supporting product version 06.1. Prepared by Earth Observation Data Centre for Water Resources Monitoring (EODC) GmbH

Holgate CM, De Jeu RAM, van Dijk AIJM et al (2016) Comparison of remotely sensed and modelled soil moisture data sets across Australia. Remote Sens Environ 186:479–500. https://doi.org/10.1016/j.rse.2016.09.015

Jackson TJ, McNairn H, Weltz MA et al (1997) First order surface roughness correction of active microwave observations for estimating soil moisture. IEEE Trans Geosci Remote Sens 35:1065–1069. https://doi.org/10.1109/36.602548

Jaeger EB, Seneviratne SI (2011) Impact of soil moisture–atmosphere coupling on European climate extremes and trends in a regional climate model. Clim Dyn 36:1919–1939. https://doi.org/10.1007/s00382-010-0780-8

Kamalanandhini M (2023) Scientometric analysis-based review of drought indices for assessment and monitoring of drought. Geogr Pannonica 27:104–118. https://doi.org/10.5937/gp27-41531

Kerr YH (2007) Soil moisture from space: where are we? Hydrogeol J 15:117–120. https://doi.org/10.1007/s10040-006-0095-3

Kim S, Liu YY, Johnson FM et al (2015) A global comparison of alternate AMSR2 soil moisture products: why do they differ? Remote Sens Environ 161:43–62. https://doi.org/10.1016/j.rse.2015.02.002

Kim S, Kim H, Choi M (2016) Evaluation of satellite-based soil moisture retrieval over the Korean Peninsula: using AMSR2 LPRM algorithm and ground measurement data. J Korea Water Resour Association 49:423–429. https://doi.org/10.3741/JKWRA.2016.49.5.423

Konopka T (2023) umap: Uniform Manifold Approximation and Projection. R package version 0.2.10.0. https://CRAN.R-project.org/package=umap. https://cran.r-project.org/web/packages/umap/index.html

Kramer PJ (1944) Soil moisture in relation to plant growth. Bot Rev 10:525–559. https://doi.org/10.1007/BF02861165

Kugler Z, Nghiem SV, Brakenridge GR (2024) SMAP passive microwave radiometer for global river flow monitoring. IEEE Trans Geosci Remote Sens 62:1–14. https://doi.org/10.1109/TGRS.2024.3359515

Kuhn M (2008) Building predictive models in *R* using the caret package. J Stat Soft. https://doi.org/10.18637/jss.v028.i05. 28:

Lakens D (2013) Calculating and reporting effect sizes to facilitate cumulative science: a practical primer for t-tests and ANOVAs. Front Psychol 26:863. https://doi.org/10.3389/fpsyg.2013.00863

Lakshmi V, Jackson TJ, Zehrfuhs D (2003) Soil moisture-temperature relationships: results from two field experiments. Hydrol Process 17:3041–3057. https://doi.org/10.1002/hyp.1275

Li Z-L, Tang R, Wan Z et al (2009) A review of current methodologies for regional evapotranspiration Estimation from remotely sensed data. Sensors 9:3801–3853. https://doi.org/10.3390/s90503801

Li X, Wigneron J-P, Frappart F et al (2020) Development and Validation of the SMOS-IC Version 2 (V2) Soil Moisture Product. In: IGARSS 2020–2020 IEEE International Geoscience and Remote Sensing Symposium. IEEE, Waikoloa, HI, USA, pp 4434–4437

Li Z-L, Leng P, Zhou C et al (2021) Soil moisture retrieval from remote sensing measurements: current knowledge and directions for the future. Earth Sci Rev 218:103673. https://doi.org/10.1016/j.earscirev.2021.103673

Liao R, Zhang S, Zhang X et al (2021) Development of smart irrigation systems based on real-time soil moisture data in a greenhouse: proof of concept. Agric Water Manage 245:106632. https://doi.org/10.1016/j.agwat.2020.106632

Liu Y, Wang Y, Zhang J (2012a) New machine learning algorithm: random forest. In: Liu B, Ma M, Chang J (eds) Information computing and applications. Springer Berlin Heidelberg, Berlin, Heidelberg, pp 246–252

Liu YY, Dorigo WA, Parinussa RM et al (2012b) Trend-preserving blending of passive and active microwave soil moisture retrievals. Remote Sens Environ 123:280–297. https://doi.org/10.1016/j.rse.2012.03.014

Liu J, Zhan X, Hain C et al (2016) NOaa Soil Moisture Operational Product System (SMOPS) and its validations. In: 2016 IEEE International Geoscience and Remote Sensing Symposium (IGARSS). IEEE, Beijing, China, pp 3477–3480

Ma H, Zeng J, Chen N et al (2019) Satellite surface soil moisture from SMAP, SMOS, AMSR2 and ESA CCI: A comprehensive assessment using global ground-based observations. Remote Sens Environ 231:111215. https://doi.org/10.1016/j.rse.2019.111215

Mauricio Zambrano-Bigiarini (2024) hzambran/hydroGOF: v0.5-4

Mazzariello A, Albano R, Lacava T et al (2023) Intercomparison of recent microwave satellite soil moisture products on European ecoregions. J Hydrol 130311. https://doi.org/10.1016/j.jhydrol.2023.130311

McColl KA, Vogelzang J, Konings AG et al (2014) Extended triple collocation: estimating errors and correlation coefficients with respect to an unknown target. Geophys Res Lett 41:6229–6236. https://doi.org/10.1002/2014GL061322

Meng X, Mao K, Meng F et al (2021) A fine-resolution soil moisture dataset for China in 2002–2018. Earth Syst Sci Data 13:3239–3261. https://doi.org/10.5194/essd-13-3239-2021

Mira NC, Catalao J, Nico G, Mateus P (2022) Soil moisture Estimation using atmospherically corrected C-Band InSAR data. IEEE Trans Geosci Remote Sens 60:1–9. https://doi.org/10.1109/TGRS.2021.3109450

Moret-Fernández D, Lera F, Latorre B et al (2022) Testing of a commercial vector network analyzer as low-cost TDR device to measure soil moisture and electrical conductivity. CATENA 218:106540. https://doi.org/10.1016/j.catena.2022.106540

Mukhlisin M, Astuti HW, Wardihani ED, Matlan SJ (2021) Techniques for ground-based soil moisture measurement: a detailed overview. Arab J Geosci. https://doi.org/10.1007/s12517-021-08263-0. 14:2032

Muñoz-Sabater J, Dutra E, Agustí-Panareda A et al (2021) ERA5-Land: a state-of-the-art global reanalysis dataset for land applications. Earth Syst Sci Data 13:4349–4383. https://doi.org/10.5194/essd-13-4349-2021

Musyimi PK, Székely B, Gandhi A, Weidinger T (2022) Palmer-type soil modelling for evapotranspiration in different Climatic regions of Kenya. HunGeoBull 71:365–382. https://doi.org/10.15201/hungeobull.71.4.4

O'Neill P, Entekhabi D, Njoku E, Kellogg K (2010) The NASA Soil Moisture Active Passive (SMAP) mission: Overview. In: 2010 IEEE International Geoscience and Remote Sensing Symposium. IEEE, Honolulu, HI, USA, pp 3236–3239

O'Neill P, Bindlish R, Chan S et al (2020) Soil moisture active passive (SMAP). Algorithm theoretical basis document level 2 & 3 soil moisture (Passive) data products. Jet Propulsion Laboratory California Institute of Technology

Owe M, De Jeu R, Holmes T (2008) Multisensor historical climatology of satellite-derived global land surface moisture. J Geophys Res 113:F01002. https://doi.org/10.1029/2007JF000769

Paruta A, Ciraolo G, Capodici F et al (2021) A Geostatistical approach to map Near-Surface soil moisture through hyperspatial resolution thermal inertia. IEEE Trans Geosci Remote Sens 59:5352–5369. https://doi.org/10.1109/TGRS.2020.3019200

Patil I (2021) Visualizations with statistical details: the Ggstatsplot approach. JOSS 6:3167. https://doi.org/10.21105/joss.03167

Pellarin T, Louvet S, Gruhier C et al (2013) A simple and effective method for correcting soil moisture and precipitation estimates using AMSR-E measurements. Remote Sens Environ 136:28–36. https://doi.org/10.1016/j.rse.2013.04.011

Portal G, Vall-llossera M, Piles M et al (2017) A spatially consistent downscaling approach for SMOS using an adaptive moving window. In: 2017 IEEE International Geoscience and Remote Sensing Symposium (IGARSS). IEEE, Fort Worth, TX, pp 4151–4153

Qiu J, Gao Q, Wang S, Su Z (2016) Comparison of Temporal trends from multiple soil moisture data sets and precipitation: the implication of irrigation on regional soil moisture trend. Int J Appl Earth Obs Geoinf 48:17–27. https://doi.org/10.1016/j.jag.2015.11.012

Rasheed MW, Tang J, Sarwar A et al (2022) Soil moisture measuring techniques and factors affecting the moisture dynamics: A comprehensive review. Sustainability 14:11538. https://doi.org/10.3390/su141811538

Ray R, Fares A, He Y, Temimi M (2017) Evaluation and inter-Comparison of satellite soil moisture products using in situ observations over Texas. U S Water 9:372. https://doi.org/10.3390/w9060372

Reinert D, Prill F, Frank H et al (2021) DWD database reference for the global and regional ICON and ICON-EPS forecasting system version 2.1.7

Reynolds SG (1970) The gravimetric method of soil moisture determination part I A study of equipment, and methodological problems. J Hydrol 11:258–273. https://doi.org/10.1016/0022-1694(70)90066-1

Rodell M, Houser PR, Jambor U et al (2004) The global land data assimilation system. Bull Amer Meteor Soc 85:381–394. https://doi.org/10.1175/BAMS-85-3-381

Saxe S, Farmer W, Driscoll J, Hogue TS (2021) Implications of model selection: a comparison of publicly available, conterminous US-extent hydrologic component estimates. Hydrol Earth Syst Sci 25:1529–1568. https://doi.org/10.5194/hess-25-1529-2021

Sazib N, Bolten JD, Mladenova IE (2022) Leveraging NASA soil moisture active passive for assessing fire susceptibility and potential impacts over Australia and California. IEEE J Sel Top Appl Earth Observations Remote Sens 15:779–787. https://doi.org/10.1109/JSTARS.2021.3136756

Scanlon T (2021) Validation of ESA CCI SM combined v06.1 vs ESA CCI SM combined v05.2 vs ERA5 v20190613

Scanlon T, Pasik A, Dorigo W et al (2021) ESA Climate Change Initiative Plus - Soil Moisture Algorithm Theoretical Baseline Document (ATBD) Supporting Product Version 06.1 D2.1 Version 2

Schmeller G, Nagy G, Sarkadi N et al (2022) Trends in extreme precipitation events (SW Hungary) based on a high-density monitoring network. HunGeoBull 71:231–247. https://doi.org/10.15201/hungeobull.71.3.2

Seneviratne SI, Corti T, Davin EL et al (2010) Investigating soil moisture–climate interactions in a changing climate: A review. Earth Sci Rev 99:125–161. https://doi.org/10.1016/j.earscirev.2010.02.004

Sheffield J (2004) A simulated soil moisture based drought analysis for the united States. J Geophys Res 109:D24108. https://doi.org/10.1029/2004JD005182

Spatafora LR, Vall-llossera M, Camps A et al (2020) Validation of SMOS L3 AND L4 soil moisture products in the remedhus (SPAIN) AND CEMADEN (BRAZIL) networks. Rev Bras Geog Fis 13:691. https://doi.org/10.26848/rbgf.v13.2.p691-712

Spennemann PC, Rivera JA, Saulo AC, Penalba OC (2015) A comparison of GLDAS soil moisture anomalies against standardized precipitation index and multisatellite estimations over South America. J Hydrometeorol 16:158–171. https://doi.org/10.1175/JHM-D-13-0190.1

Sun X, Lai P, Wang S et al (2022) Monitoring of extreme agricultural drought of the past 20 years in Southwest China using GLDAS soil moisture. Remote Sens 14:1323. https://doi.org/10.3390/rs14061323

Sure A, Dikshit O (2022) Combined radiometer and scatterometer derived soil moisture product for the Indo-Gangetic basin. Geocarto Int 37:456–473. https://doi.org/10.1080/10106049.2020.1720313

Todd W, Hoffer SMR (1998) Responses of spectral indices to variations in vegetation cover and soil background. Photogram Eng Remote Sens 64:915–922

Togneri R, Felipe Dos Santos D, Camponogara G et al (2022) Soil moisture forecast for smart irrigation: the primetime for machine learning. Expert Syst Appl 207:117653. https://doi.org/10.1016/j.eswa.2022.117653

Ulaby FT, Aslam A, Dobson MC (1982) Effects of vegetation cover on the radar sensitivity to soil moisture. IEEE Trans Geosci Remote Sens GE –20:476–481. https://doi.org/10.1109/TGRS.1982.350413

Unnikrishnan CK, George JP, Lodh A et al (2016) Validation of two gridded soil moisture products over India with in-situ

observations. J Earth Syst Sci 125:935–944. https://doi.org/10.1007/s12040-016-0714-x

Veihmeyer FJ, Hendrickson AH (1950) Soil moisture in relation to plant growth. Annu Rev Plant Physiol 1:285–304. https://doi.org/10.1146/annurev.pp.01.060150.001441

Verhoest N, Lievens H, Wagner W et al (2008) On the soil roughness parameterization problem in soil moisture retrieval of bare surfaces from synthetic aperture radar. Sensors 8:4213–4248. https://doi.org/10.3390/s8074213

Wang G, Garcia D, Liu Y et al (2012) A three-dimensional gap filling method for large geophysical datasets: application to global satellite soil moisture observations. Environ Model Softw 30:139–142. https://doi.org/10.1016/j.envsoft.2011.10.015

Wang X, Wang B, Xu X et al (2018) Spatial and Temporal variations in surface soil moisture and vegetation cover in the loess plateau from 2000 to 2015. Ecol Ind 95:320–330. https://doi.org/10.1016/j.ecolind.2018.07.058

Wen X, Lu H, Li C et al (2014) In: Jackson TJ, Chen JM, Gong P, Liang S (eds) Inter-comparison of soil moisture products from SMOS, AMSR-E, ECWMF and GLDAS over the Mongolia plateau. Beijing, China, p 92600O

Wigneron J-P, Li X, Frappart F et al (2021) SMOS-IC data record of soil moisture and L-VOD: historical development, applications and perspectives. Remote Sens Environ 254:112238. https://doi.org/10.1016/j.rse.2020.112238

Yang G, Guo P, Li X et al (2020) Assessment with remotely sensed soil moisture products and ground-based observations over three dense network. Earth Sci Inf 13:663–679. https://doi.org/10.1007/s12145-020-00454-9

Yang L, Wei W, Wang T, Li L (2022) Temporal-spatial variations of vegetation cover and surface soil moisture in the growing season across the mountain-oasis-desert system in Xinjiang, China. Geocarto Int 37:3912–3940. https://doi.org/10.1080/10106049.2021.1871666

Yee MS, Walker JP, Rüdiger C et al (2017) A comparison of SMOS and AMSR2 soil moisture using representative sites of the OzNet monitoring network. Remote Sens Environ 195:297–312. https://doi.org/10.1016/j.rse.2017.04.019

Yin J, Zhan X, Liu J (2020) NOAA satellite soil moisture operational product system (SMOPS) version 3.0 generates higher accuracy blended satellite soil moisture. Remote Sens 12:2861. https://doi.org/10.3390/rs12172861

Yin J, Zhan X, Liu J, Ferraro RR (2022) A new method for generating the SMOPS blended satellite soil moisture data product without relying on a model climatology. Remote Sens 14:1700. https://doi.org/10.3390/rs14071700

Zhan X, Liu J, Zhao L (2016) Noaa Nesdis center for satellite applications and research. Soil moisture operational product system (Smops). Algorithm Theoretical Basis Document Version 4.0.

Zhang Y-K, Schilling KE (2006) Effects of land cover on water table, soil moisture, evapotranspiration, and groundwater recharge: A field observation and analysis. J Hydrol 319:328–338. https://doi.org/10.1016/j.jhydrol.2005.06.044

Zhang Y, Liang S, Ma H et al (2023) Generation of global 1 Km daily soil moisture product from 2000 to 2020 using ensemble learning. Earth Syst Sci Data 15:2055–2079. https://doi.org/10.5194/essd-15-2055-2023

Zheng W, Zhan X, Liu J, Ek M (2018) A preliminary assessment of the impact of assimilating satellite soil moisture data products on NCEP global forecast system. Adv Meteorol 2018:1–12. https://doi.org/10.1155/2018/7363194

Zheng X, Feng Z, Li L et al (2021) Simultaneously estimating surface soil moisture and roughness of bare soils by combining optical and radar data. Int J Appl Earth Obs Geoinf 100:102345. https://doi.org/10.1016/j.jag.2021.102345

Zheng J, Zhao T, Lü H et al (2022) Assessment of 24 soil moisture datasets using a new in situ network in the Shandian river basin of China. Remote Sens Environ 271:112891. https://doi.org/10.1016/j.rse.2022.112891